Article

SOURCE DATA | TRANSPARENT PROCESS | OPEN ACCESS

THE EMBO JOURNAL

Histone retention preserves epigenetic marks during heat stress-induced transcriptional memory in plants

Loris Pratx[1], Philipp Wendering[2,3], Christian Kappel[4], Zoran Nikoloski[2,3] & Isabel Bäurle[1,*]

Abstract

Plants often experience recurrent stressful events, for example, during heat waves. They can be primed by heat stress (HS) to improve the survival of more severe heat stress conditions. At certain genes, sustained expression is induced for several days beyond the initial heat stress. This transcriptional memory is associated with hypermethylation of histone H3 lysine 4 (H3K4me3), but it is unclear how this is maintained for extended periods. Here, we determined histone turnover by measuring the chromatin association of HS-induced histone H3.3. Genome-wide histone turnover was not homogenous; in particular, H3.3 was retained longer at heat stress memory genes compared to HS-induced non-memory genes during the memory phase. While low nucleosome turnover retained H3K4 methylation, methylation loss did not affect turnover, suggesting that low nucleosome turnover sustains H3K4 methylation, but not vice versa. Together, our results unveil the modulation of histone turnover as a mechanism to retain environmentally mediated epigenetic modifications.

Keywords heat stress; histone retention; histone turnover; priming; transcriptional memory

Subject Categories Chromatin, Transcription & Genomics; Plant Biology

DOI 10.15252/embj.2023113595 | Received 24 January 2023 | Revised 19 October 2023 | Accepted 19 October 2023 | Published online 8 November 2023

The EMBO Journal (2023) 42: e113595

Introduction

Adverse environmental conditions interfere with plant growth and development and are referred to as stress. Plants can plastically respond to stress conditions; for instance, priming after a transient stress cue modifies responses to a recurrent stress after a stress-free interval (Conrath, 2011; Hilker *et al*, 2016; Lämke & Bäurle, 2017). Such somatic stress memory is activated by a number of different biotic and abiotic stressors (Jaskiewicz *et al*, 2011; Ding *et al*, 2012; Conrath *et al*, 2015; Feng *et al*, 2016; Lämke *et al*, 2016; Bäurle, 2017; Lämke & Bäurle, 2017). A hallmark of somatic stress memory is a transcriptional memory, which is apparent from either enhanced re-induction of stress-induced genes following a second stress exposure or from the sustained induction of stress-induced genes that extends considerably beyond the duration of the stress cue (Bäurle, 2017). Chromatin modifications, in particular histone H3 lysine 4 (H3K4) methylation, have been associated with transcriptional stress memory and are instrumental in modifying re-induction patterns (Jaskiewicz *et al*, 2011; Ding *et al*, 2012; Singh *et al*, 2014; Feng *et al*, 2016; Oberkofler & Bäurle, 2022).

Heat stress (HS) is a major constraint to global crop yields and is predicted to increase with climate change (Battisti & Naylor, 2009; Lobell *et al*, 2011). The acute HS response in plants is similar to that of yeast and metazoans (Richter *et al*, 2010; Li *et al*, 2017; Ohama *et al*, 2017; Gomez-Pastor *et al*, 2018). Heat shock transcription factors (HSFs) are activated in response to HS and induce the expression of heat shock protein (HSP) chaperones to maintain proteostasis. HS primes plants for an improved response to a recurrent HS (Charng *et al*, 2006, 2007; Lämke & Bäurle, 2017). This HS memory results in enhanced survival upon a recurrent HS that would be lethal to a naïve plant (Charng *et al*, 2006; Stief *et al*, 2014; Brzezinka *et al*, 2016). The components that mediate HS memory are distinct from those of the acute HS response and are beginning to be unraveled (Charng *et al*, 2006, 2007; Stief *et al*, 2014; Brzezinka *et al*, 2016, 2019; Friedrich *et al*, 2021; Oberkofler *et al*, 2021). Two so-called memory HSFs, HSFA2 and HSFA3, are induced after HS and amplify the induction of a subset of HS response genes (Charng *et al*, 2007; Liu *et al*, 2011; Nishizawa-Yokoi *et al*, 2011; Lämke *et al*, 2016; Friedrich *et al*, 2021). Many of these, including *ASCORBATE PEROXIDASE2* (*APX2*), *HEAT-SHOCK ASSOCIATED32* (*HSA32*), *HSP22.0*, and *HSP18.2*, have been classified as HS memory genes due to their sustained induction after HS (Friedrich *et al*, 2021). HSFA2 binds HS memory genes transiently; however, HSFA2-dependent transcriptional induction is more extended (Lämke *et al*, 2016). In contrast, HS-induced non-memory genes, for example, *HSP70* and *HSP101*, show a rapid loss of induction during recovery.

Memory HSFs induce histone H3 lysine 4 (H3K4) hypermethylation at HS memory genes, and this remains elevated for the

1 Plant Epigenetics, Institute for Biochemistry and Biology, University of Potsdam, Potsdam, Germany
2 Bioinformatics, Institute for Biochemistry and Biology, University of Potsdam, Potsdam, Germany
3 Systems Biology and Mathematical Modeling Group, Max Planck Institute of Molecular Plant Physiology, Potsdam, Germany
4 Genetics, Institute for Biochemistry and Biology, University of Potsdam, Potsdam, Germany
*Corresponding author. Tel: +49 331 9775581; E-mail: isabel.baeurle@uni-potsdam.de

duration of the memory phase (Lämke *et al*, 2016; Liu *et al*, 2018; Friedrich *et al*, 2021), suggesting a function of this HS-induced epigenetic modification in extending the duration of active transcription. Thus, the current model is that HSFA2/HSFA3 mediate transcriptional memory through H3K4 hyper-methylation (Lämke *et al*, 2016; Oberkofler & Bäurle, 2022). However, the mechanism by which HSFA2/HSFA3 mediate sustained H3K4 hyper-methylation is unknown, as is the identity of the histone methyltransferase (HMT) that writes H3K4 hyper-methylation during HS memory. While *SET DOMAIN PROTEIN 25* (*SDG25*) and *ARABIDOPSIS TRITHORAX HOMOLOG 1* (*ATX1*) have been implicated in HS-induced H3K4me3, it is not known whether they target HS memory genes (Song *et al*, 2021). In yeast and mammalian cells, H3K4 hyper-methylation marks recent transcriptional activity of a locus and causes modified reactivation after a second stimulus (Ng *et al*, 2003; D'Urso *et al*, 2016).

Together with nucleosome occupancy, histone modifications regulate the accessibility of chromatin for transcription. Writer and eraser enzymes dynamically regulate histone modifications, including methylation and acetylation, primarily on the N-terminal tails of histones H3 and H4. Transcription, but also replication, recombination, and DNA damage repair involve the temporary dissolving of nucleosomal structures, thus affecting the inheritance and stability of posttranslational histone modifications. Nucleosome turnover was profiled in yeast and metazoans with induced tagged histones, revealing the highest exchange rates at promoters and enhancers of active genes, and an overall (but not necessarily linear) association with expression strength (Dion *et al*, 2007; Rufiange *et al*, 2007; Deal *et al*, 2010; Kraushaar *et al*, 2013; Deaton *et al*, 2016; Storck *et al*, 2020; Yaakov *et al*, 2021). Histone chaperones such as FACILITATES CHROMATIN TRANSCRIPTION (FACT) and SUPPRESSOR OF TY6 (SPT6) recycle nucleosomes during transcription and thus maintain histone modifications (Jeronimo *et al*, 2019; Murawska *et al*, 2021).

A major unresolved question is how HS-induced H3K4 hyper-methylation is maintained through the memory phase, especially at a time when HSFA2 has dissociated from the locus. Histone modifications may be retained by increasing the fidelity with which a modified nucleosome is recycled at the same position after replication or passage of RNA polymerase II, leading in effect to a lower histone turnover at these loci. Here, we examine this possibility by estimating histone turnover using pulse-labeled histone H3.3. Our results show that histone turnover rates are lower for HS memory-related genes compared to HS-induced non-memory genes or genes that do not change expression. In particular, H3K4me3-marked histones are strongly retained. Thus, our study provides a tentative mechanism for how elevated histone methylation is maintained during active somatic stress memory.

Results

HS-induced GFP-Histone H3.3 is detected for 72 h after HS

To study histone turnover dynamics after HS in *Arabidopsis thaliana*, we generated transgenic plants expressing GFP-tagged histone H3.3 (*HTR5*) under control of the HS-inducible *HSP21* promoter (Fig 1A) (Stief *et al*, 2014; Oberkofler & Bäurle, 2022). H3.3-GFP fusion proteins have been used previously to assess H3.3 dynamics in plants and other systems, and those studies concluded that the size of the GFP moiety did not affect H3.3 dynamics (Goldberg *et al*, 2010; Wollmann *et al*, 2012; Shu *et al*, 2014; Otero *et al*, 2016; Zhao *et al*, 2022). Transgene expression was assessed on 5-day-old seedlings before and after HS by qRT–PCR (Fig 1B and C) and was significantly induced at 4 h after HS. While we could not detect H3.3-GFP protein with anti-H3 antibodies, we could detect it with anti-GFP by immunoblotting. H3.3-GFP was undetectable before HS, strongly induced 4 h after HS, and remained detectable for at least 3 days (72 h) of recovery at normal growth temperature (Fig 1D). Likewise, GFP fluorescence was observed in all tissues with highest intensity at 4 h of recovery (Fig EV1), indicating that the *HSP21* promoter is activated in all tissues. For comparison, in *Drosophila melanogaster* soluble H3.3 was present for up to 8 h after induction and the genome-wide half-life of chromatinized H3.3 was around 24 h (Schwartz & Ahmad, 2005).

We next tested whether anti-H3 recognized H3.3-GFP during chromatin immunoprecipitation (ChIP) by performing sequential ChIP analysis, where we successively applied anti-H3 or anti-GFP followed by anti-H3, anti-GFP, or IgG (negative control) (Fig 1E). Independently of the order of application, sequential ChIP with anti-H3 and anti-GFP precipitated similar amounts of chromatin as the successive use of only anti-GFP, indicating that anti-H3 recognizes H3.3-GFP as efficiently as anti-GFP in ChIP.

H3.3-GFP association is similar between HS memory and non-memory genes

To investigate whether histone turnover dynamics contribute to transcriptional memory after HS, we studied the incorporation and loss of H3.3-GFP after HS at several HS-induced loci. H3.3-GFP is highly abundant shortly after HS (Figs 1D and EV1). Genes with a high histone turnover rate are expected to integrate more H3.3-GFP during this stage (Fig 2A). Consequently, during the early phase after HS, high turnover loci are expected to integrate more H3.3-GFP than low histone turnover loci. Conversely, during the late/memory phase when free H3.3-GFP is no longer available, H3.3-GFP will be replaced more quickly with untagged histones at high turnover loci than at low turnover loci. During the memory phase, high turnover loci are expected to lose GFP signal faster than low turnover loci. Thus, high turnover loci will exhibit a higher GFP peak that disappears quickly, while low histone turnover loci will show a lower GFP peak that is maintained for longer.

We investigated H3.3-GFP integration relative to total H3 in a time course from 4 h to 72 h after the end of HS (Fig 2C, Appendix Fig S1). We analyzed eight different loci at seven time points (Fig 2B); *ACTIN7* (*ACT7*) was selected as a euchromatic expressed gene with expected high histone turnover and *AtGP* as a heterochromatic retroelement with low histone turnover (Zhang *et al*, 2018). The six analyzed HS response genes included *HSP101* and *HSP70* as HS-induced non-memory genes, and *HSP22*, *HSP18.2*, *APX2*, and *HSA32* as HS memory genes (Lämke *et al*, 2016). We estimated the respective peak of H3.3-GFP integration from the enrichment of H3.3-GFP at 4 h after HS, when H3.3-GFP protein levels peaked (Fig 1D). In line with our expectations, *AtGP* showed less H3.3-GFP enrichment than *ACT*, suggesting that *ACT* has a higher histone turnover (Fig 2C). Moreover, three of the four memory genes (i.e., *HSP18.2*, *APX2*, and *HSA32*) showed similar H3.3-GFP levels as the

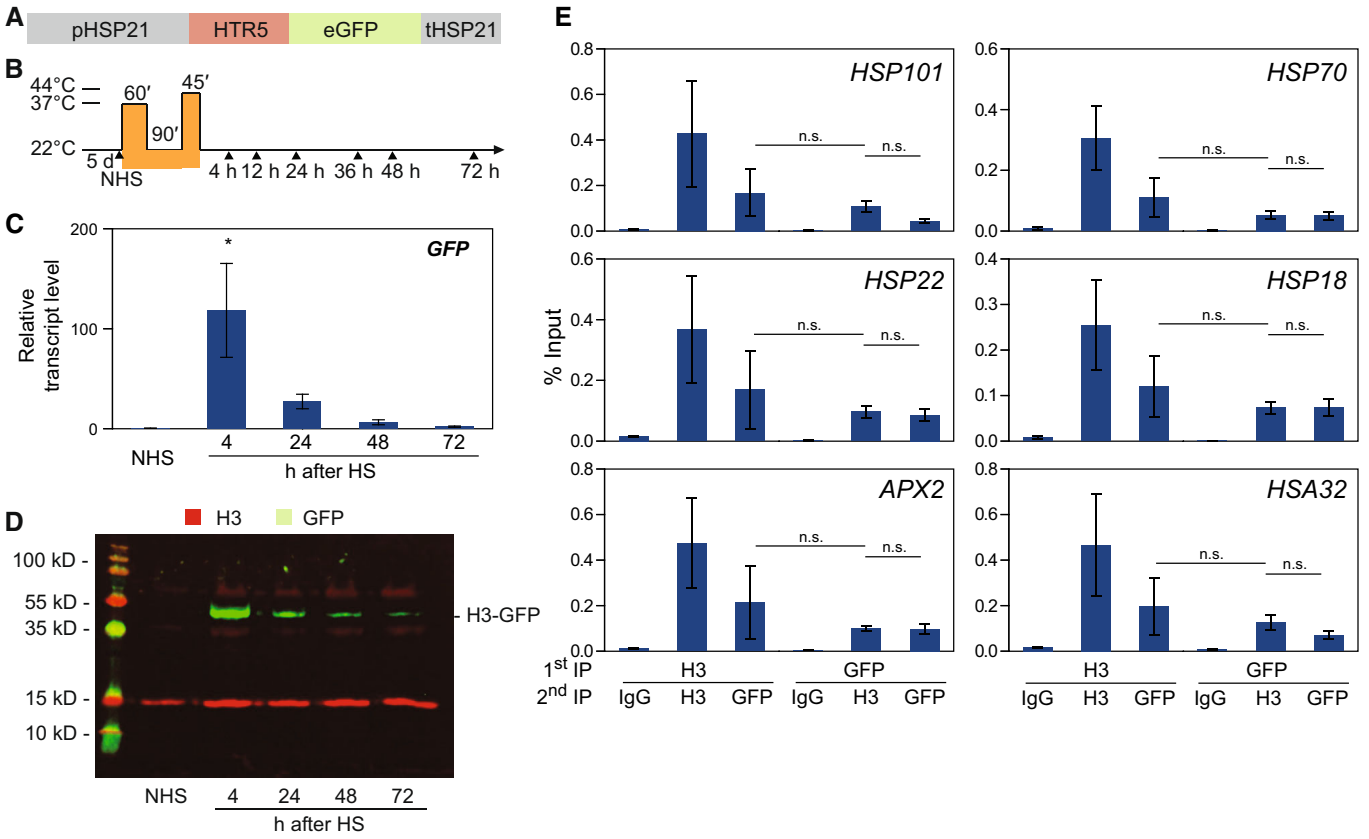

Figure 1. Characterization of a HS-inducible H3.3-GFP line for profiling H3 turnover.

A Schematic of histone *H3.3 (HTR5)–eGFP* fusion construct driven by the HS-inducible *HSP21* promoter (*pHSP21*) and endogenous terminator (*tHSP21*).

B Treatment scheme for HS assays. 5-day-old seedlings were subjected to the indicated treatments and sampled between 4 and 72 h after the end of the treatment.

C Transcript levels of H3.3-GFP determined by qRT–PCR at different recovery times after HS relative to the *At4g26410* reference. Data are mean ± s.e.m. of three biological replicates. Asterisk indicates statistically significant difference relative to NHS ($P < 0.05$, unpaired, two-sided *t*-test).

D Immunoblotting of H3.3-GFP (44 kDa) samples at different time points after HS. The signal is maximal at 4 h after HS and still detectable at 72 h. Anti-H3 signal is detected for the endogenous H3 (17 kDa), but not H3.3-GFP. Results from one representative experiment are shown.

E Sequential ChIP-qPCR indicates that anti-H3 detects H3.3-GFP in ChIP. Chromatin of H3.3-GFP seedlings 4 h after HS was immunoprecipitated by two (different) antibodies as indicated, including anti-H3, anti-GFP, and IgG (negative control). Similar recovery percentages were found in samples immunoprecipitated with anti-H3 and then anti-GFP, anti-GFP and then anti-H3, or successive usage of only anti-GFP. Data shown are mean enrichment relative to Input ± s.e.m. at the indicated genes (cf. Fig 2B) of three biological replicates. n.s., not significantly different ($P > 0.05$) using *t*-test.

Source data are available online for this figure.

non-memory genes *ACT*, *HSP101*, and *HSP70*, suggesting that H3.3-GFP integration, and thus histone turnover, during the early phase was the same. Thus, during the early phase after HS, memory genes did not differ in histone turnover from HS-inducible non-memory genes or highly expressed genes.

H3.3-GFP dissociation dynamics differ between HS memory and non-memory genes

At the transcriptional level, HS memory is evident for several days after the end of HS, and hence, differences in histone turnover may only become apparent during the memory phase. Thus, we analyzed the retention of H3.3-GFP during this phase (Fig 2C, Appendix Fig S1). GFP enrichment declined at all loci starting from 12 h (Fig 2C and D). To better compare the H3.3-GFP dynamics, we fitted an exponential decay function to the time-course data, normalizing all signal values to the H3.3-GFP signal at 4 h (Fig 2D and E, Appendix Fig S2). For all tested loci, the models showed a good fit to the experimental data (Appendix Table S1). We estimated the decay constant representing the kinetics of H3.3-GFP turnover from the curves of each locus (Fig 2F, Appendix Fig S2). Three of four memory genes (*HSP18*, *APX2*, and *HSA32*) displayed significantly smaller decay constants compared to the non-memory genes *ACT*, *HSP101*, and *HSP70*. The *HSP22* memory gene displayed a statistically significant smaller decay constant than *HSP101*, but not *ACT* or *HSP70*. In summary, our findings indicate that during the memory phase HS memory genes show a reduced histone turnover compared to non-memory genes.

To confirm our findings at the genome-wide level, we performed ChIP-sequencing with total H3 and H3.3-GFP at 4 and 24 h after HS, respectively, and non-HS control. According to a previous definition of HS memory genes (Friedrich *et al*, 2021), we determined the

average signal for genes that are upregulated early and late after HS (4–52 h after HS) and compared them to genes that are induced only early after HS (up to 4 or 28 h) and to all other genes. Over all groups, total H3 profiles peaked in the gene body with low signal over the TSS and TTS regions (Figs 3A and EV2A). In contrast, H3.3-GFP profiles after HS were higher in the gene body of memory genes compared to all other genes, as evidenced also from the empirical cumulative distribution function of H3.3-GFP in the TSS + 200 bp to TSS + 700 bp interval (Figs 3A and B, EV2A and B). GFP signal in the promoter was similar between memory genes and early HS genes, suggesting that turnover was specifically regulated in transcribed regions. For all genes and especially for early HS genes, H3.3-GFP peaked around the 3′ end of genes (Fig 3A). Although our analysis did not determine steady-state H3.3 levels, our findings are consistent with the previously reported genome-wide localization of H3.3 (Stroud *et al*, 2012; Shu *et al*, 2014; Zhao *et al*, 2022). The increased GFP signal in the transcribed region of memory genes is consistent with the notion that memory genes have reduced histone turnover during the memory phase and that this contributes to their transcriptional memory.

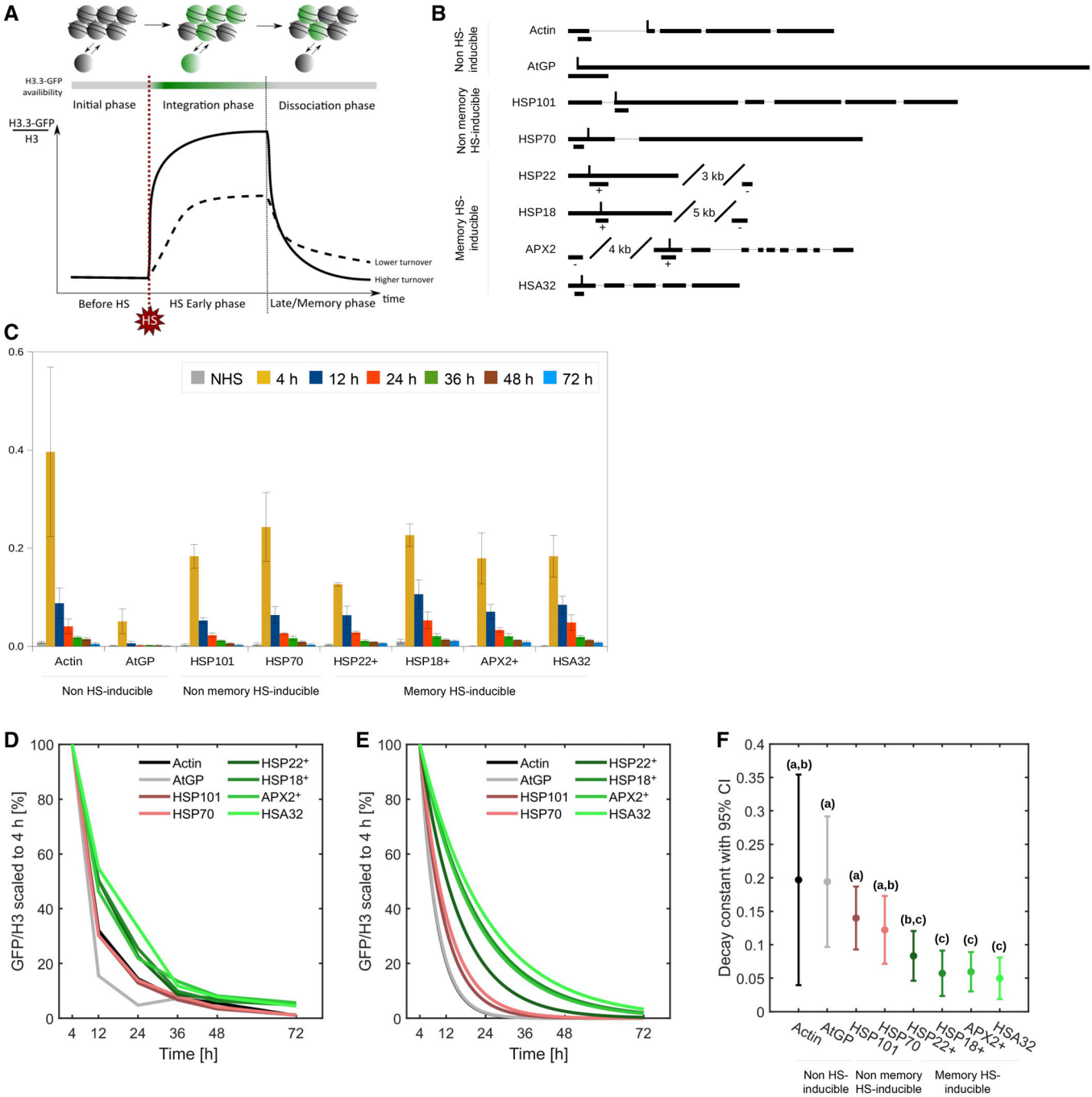

Figure 2.

Figure 2. H3.3-GFP incorporation and dissociation patterns after HS and modeling of turnover dynamics.

A Before HS, H3.3-GFP (green) is not expressed and the chromatin contains only non-tagged histones (gray). During the early phase after HS, H3.3-GFP is strongly induced and is integrated into the chromatin globally. Regions with higher histone turnover exhibit a higher GFP peak due to a rapid and comprehensive replacement of untagged H3 with H3.3-GFP. During the Late/Memory phase, free H3.3-GFP is no longer available. H3.3-GFP signal at loci with high histone turnover declines more rapidly due to replacement of the H3.3-GFP with untagged H3.

B Localization of amplicons for the ChIP-qPCR assays. *ACT* was selected as an expressed gene. *AtGP* is a gene with low turnover. *HSP101* and *HSP70* are HS-induced non-memory genes. *HSP22*, *HSP18*, *APX2*, and *HSA32* are memory genes. Vertical bar indicates localization of the ATG.

C–F H3.3-GFP association and dissociation after HS at the indicated loci as determined by ChIP-qPCR on H3.3-GFP seedlings without HS (NHS), and 4, 12, 24, 36, 48, and 72 h after HS. (C) Dynamics of H3.3-GFP enrichment relative to total H3. The GFP/H3 ratio at 4 h was used to estimate histone turnover during the early phase. Data shown are means ± s.e.m. of three biological replicates. (D–F) Dynamics of H3.3-GFP dissociation were determined as percentage of GFP/H3. For each locus, GFP/H3 values were normalized to the 4 h value to represent the relative decline of integrated H3.3-GFP at later time points (D). These data were used to fit an exponential decay function (E) and derive dissociation constants for each locus as an estimate of histone turnover (F). For three out of four tested memory genes (i.e., *HSP18*$^+$, *APX2*$^+$, and *HSA32*), the decay constant was statistically lower than that of the tested non-memory genes (i.e., *ACT*, *HSP101*, and *HSP70*). For the fourth memory gene *HSP22*$^+$, the decay constant was lower than that of *HSP101*. Data shown are means of three biological replicates ± 95% confidence interval (CI). Different letters indicate statistically significant difference ($P < 0.05$, *t*-test with Benjamini–Hochberg correction).

Source data are available online for this figure.

Interestingly, this pattern appears to be in place already at 4 h after HS.

Histone retention correlates with retention of H3K4me3 but not of H3K9ac

HS memory is correlated with sustained hyper-methylation of H3K4me3 (Lämke *et al*, 2016; Liu *et al*, 2018). Our previously published patterns of H3K4me3 enrichment (Lämke *et al*, 2016; Friedrich *et al*, 2021) suggest H3K4me3 accumulates in the gene body near the TSS. This is also consistent with the general distribution of H3K4me3 along all genes (Roudier *et al*, 2011). In addition, HS induces acetylation of H3K9 at these genes; however, the presence of this modification is more restricted to the period of active transcription. With HS memory genes exhibiting lower histone turnover during the memory phase, the retention of histones and histone modifications may be linked. We thus hypothesized that during the memory phase retained (H3.3-GFP) histones are enriched in histone modifications compared to the global pool of H3 histones.

To test this hypothesis, we performed sequential ChIP at 24 and 48 h after HS using either anti-H3 or anti-GFP antibodies followed by anti-H3K4me3 or anti-H3K9ac antibodies, respectively (Fig 4). HS memory genes showed a consistent enrichment in H3K4me3 and H3K9ac at 24 and 48 h, in accordance with previous findings (Lämke *et al*, 2016). This enrichment was not present in control amplicons that were located 3–5 kb away from *HSP22*, *HSP18.2*, and *APX2* (denoted *HSP22neg*, *HPS18neg*, and *APX2neg*) (Lämke *et al*, 2016; Friedrich *et al*, 2021). At memory genes, the methylation and acetylation marks were more highly enriched in retained H3.3-GFP compared to all histone H3 at 24 and 48 h (between 3x and 16x). H3K4 methylation was more highly enriched in retained H3.3-GFP compared to all histone H3 in all memory genes at 24 h, and in *HSP22* and *APX2* also at 48 h. By contrast, acetylation was distributed more uniformly between H3.3-GFP and all histone H3 and did not show a statistically significant difference in enrichment except for *HSA32* at 24 h. These data support the existence of a link between histone retention and sustained histone modification.

To quantify the potential correlation between the retention of histones and their modifications, we repeated the experiment at 4 and 24 h after HS (Fig EV3). Consistent with the previous analysis, the enrichment of methylated and acetylated H3 was higher in H3.3-GFP compared to all H3 histones for memory genes at 24 h after HS. As total levels of H3.3-GFP (free and chromatin-bound) decreased rapidly after 4 h (Fig 1A), the majority of methylated H3.3-GFP at 24 h likely originated from retained histones. At 4 h after HS, methylation and acetylation levels were similar between H3.3-GFP and total histone H3 at all loci. From these data, we calculated a methylation/acetylation factor to estimate the contribution of histone retention to the total methylation/acetylation levels. To calculate the methylation factor F, first, we calculated the difference between the fraction of methylation on retained histones (estimated as H3.3-GFP, cf. Materials and Methods) and the fraction of methylation on *de novo* deposited histones (estimated as total H3 minus H3.3-GFP, cf. Materials and Methods) and then divided this difference by the fraction of methylation at 4 h. The methylation factor was higher (and positive) for memory genes (between 2.55 and 4.26) compared to non-memory genes (between −0.54 and 0.51) (Fig 5A, Appendix Fig S3A). The negative correlation (Pearson correlation coefficient: −0.83) between histone decay and methylation factor indicates that lower turnover is associated with higher contribution of H3K4me3 on retained histones toward total H3K4me3.

In an analogous manner, to calculate the acetylation factor we divided the difference between the fraction of acetylation on retained histones (estimated as H3.3-GFP, cf. Materials and Methods) and the fraction of acetylation on *de novo* deposited histones (estimated as total H3 minus H3.3-GFP, cf. Materials and Methods) by the fraction of acetylation at 4 h. In comparison to the methylation factor, the acetylation factor showed overall no difference between memory genes (between 2.56 and 5.29) and non-memory genes (between 1.84 and 2.98) (Fig 5B). The differences in the acetylation factor varied between biological replicates, with three of five replicates supporting higher acetylation factors for memory genes and two of five replicates supporting the opposite pattern (Appendix Fig S3B). In addition, there was no apparent trend between the acetylation factor and histone turnover. Thus, our findings suggest that H3K4me3, but not H3K9ac, correlates with the retention of histones. Notably, we also did not find a correlation between histone turnover and gene expression levels after HS at corresponding time points (Fig EV4).

To further investigate the relationship between H3K4me3, transcriptional activity, and histone dynamics, we analyzed H3.3-GFP decay dynamics in *hsfa2* mutants that have strongly reduced H3K4me3 and loss of transcriptional activity during the later stages after HS (Lämke *et al*, 2016). *Hsfa2* mutants still maintained significantly reduced nucleosome turnover at HS memory genes *HSP18.2*,

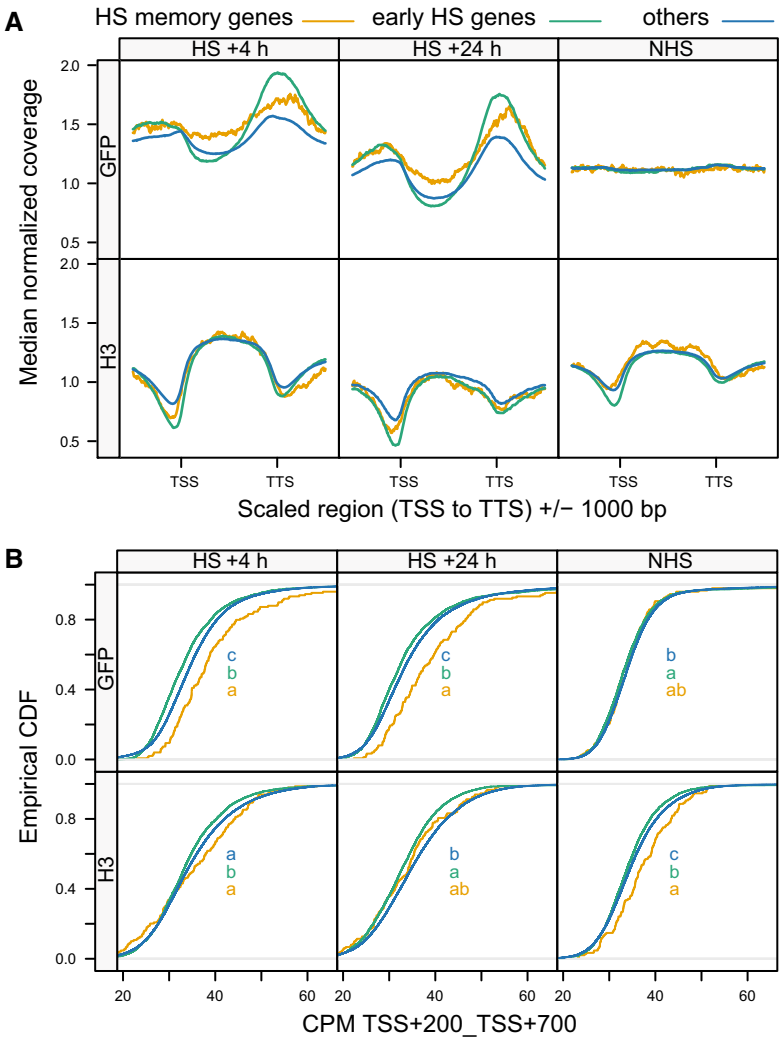

Figure 3. Global average coverage profiles of H3.3-GFP and H3 at memory and non-memory genes.

The global distribution of H3.3-GFP during the memory phase was determined by ChIP-seq on H3.3-GFP seedlings without HS (NHS) or 4 or 24 h after HS with anti-H3 or anti-GFP, respectively.

A Mean normalized coverage was plotted per replicate for H3.3-GFP (retained histones) or H3 (global pool of histones) between TSS and TTS ± 1 kb for different gene groups (HS memory genes, early HS genes, and all other genes). While the H3 profiles are similar between groups, H3.3-GFP signal in the gene body is higher in HS memory genes after HS, but not NHS, suggesting that H3.3-GFP histones are retained during HS memory.

B Empirical cumulative distribution function displaying the coverage (counts per million, cpm) for the indicated groups and samples in the region TSS + 200 bp to TSS + 700 bp. Different letters indicate significant differences ($P < 0.05$, KS test).

Data information: Data are averaged over three biological replicates (cf. Fig EV2).
Source data are available online for this figure.

APX2, and *HSA32* compared to non-memory genes (Fig EV5). Thus, reduced nucleosome turnover is not mediated by H3K4me3, supporting the notion that low turnover sustains H3K4me3 and not *vice versa*.

Discussion

HS responses of *A. thaliana* can be divided into an early and a late/memory phase. During the early phase, HS-induced genes are highly transcribed and histone turnover is high. This is in line with previous findings that gene activation increases histone turnover (Deal *et al*, 2010; Deaton *et al*, 2016). During the memory phase, HS-induced non-memory genes are shut down, while transcription of memory-related genes remains elevated, and so do H3K4me3 levels. A major question is how this hyper-methylation is maintained during the memory phase. In principle, the continuous recruitment of HMTs could maintain hyper-methylation. Alternatively, reduced histone turnover may maintain hyper-methylation. Our findings support the latter model as we observe globally lower histone turnover at HS memory genes compared to HS-induced non-memory genes during the memory phase.

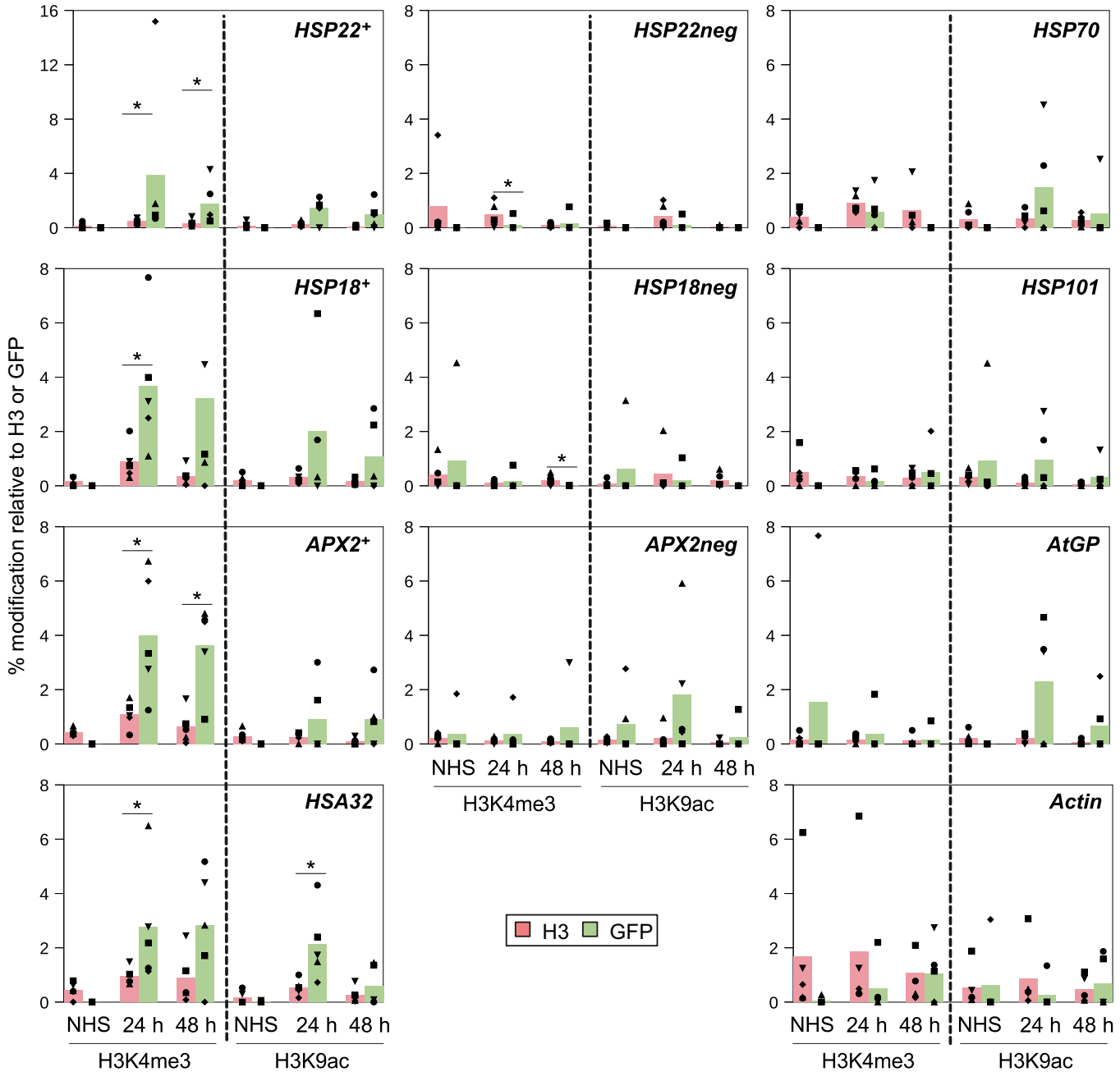

Figure 4. After HS H3K4me3 is enriched on retained H3.3-GFP compared to the total pool of H3.

Enrichment of H3K4me3 and H3K9ac on H3 incorporated during the HS response (GFP, green) and on total histone H3 (red), respectively. Enrichment at the indicated loci (neg denotes control region several kb away from the indicated gene) was determined by sequential ChIP-qPCR without HS (NHS), or 24 and 48 h after HS, respectively. Chromatin was immunoprecipitated with anti-H3 or anti-GFP antibodies followed by anti-H3K4me3, anti-H3K9ac, or IgG (negative control) antibodies. The percentage of histone modifications among H3 or GFP was calculated. To control for variation in ChIP efficiency between replicates, each replicate was normalized to the average signal from that replicate (overall measured amplicons). At memory genes, the relative enrichment of H3K4me3 is higher in retained histones than in the total pool of histones. Data shown are means and individual data points of five biological replicates. Asterisks indicate significant differences between H3 and GFP ($P < 0.05$, Wilcoxon Mann–Whitney test).

Source data are available online for this figure.

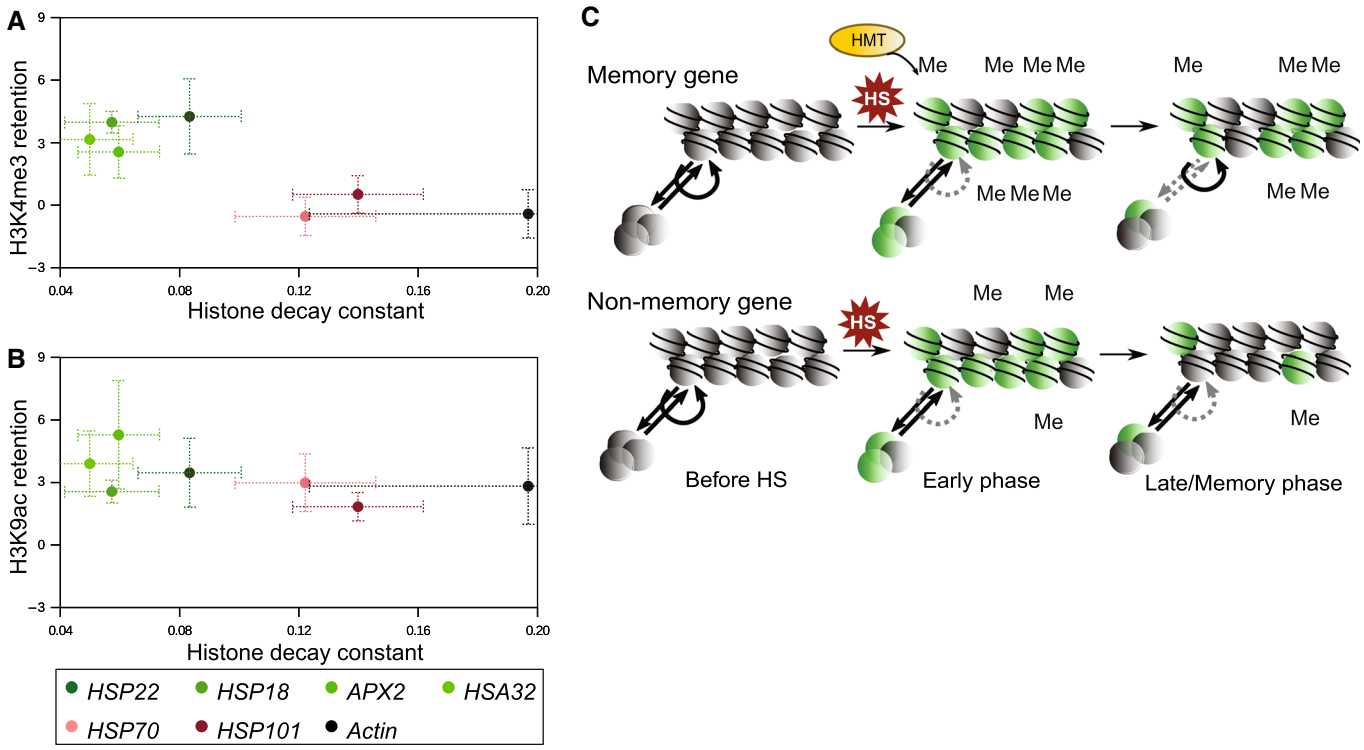

Figure 5. Involvement of histone turnover in stabilizing H3K4me3 and H3K9ac during HS memory.

A, B From the enrichment of H3K4me3 (A) or H3K9ac (B) among retained (H3.3-GFP) or total histones (H3), a modification retention factor was calculated for every locus and plotted against the histone decay constant (cf. Fig 2F). H3K4me3 correlates negatively with histone decay, and memory genes (green) exhibit a higher H3K4me3 retention factor than non-memory genes (red). H3K9ac and histone decay were not correlated. Data shown are means ± s.e.m. of five biological replicates (cf. Appendix Fig S3).

C Model for the involvement of histone turnover in epigenetic HS memory. Among memory genes, histones integrated during the early phase after HS (green) are methylated by histone methyltransferases (HMT) to generate H3K4me3 (Me). During the memory phase, increased nucleosome recycling retains H3K4me3-modified histones, and thus maintains high H3K4me3. By contrast, at non-memory genes nucleosomes are more rapidly replaced and H3K4 methylation turned over.

Source data are available online for this figure.

To our knowledge, we provide the first report of histone turnover in plants. Histone turnover is not homogenous as we observed a lower H3.3-GFP integration at an inactive locus (*AtGP*) relative to active loci (*ACT*, *HSP101*, *HSP70*, *HSP18*, *APX2*, and *HSA32*). This is in overall accordance with studies in fungi and metazoans that suggest that histone turnover is higher at expressed loci, especially in promoters and enhancers (Dion *et al*, 2007; Rufiange *et al*, 2007; Deal *et al*, 2010; Kraushaar *et al*, 2013; Svensson *et al*, 2015; Deaton *et al*, 2016; Storck *et al*, 2020; Yaakov *et al*, 2021). However, histone turnover did not quantitatively correlate with expression levels after HS, supporting the notion that there is no simple connection between pre-initiation complex assembly and histone turnover, but rather an involvement of gene-specific regulators (Deaton *et al*, 2016; Kassem *et al*, 2020). Our global analysis indicates that lower histone turnover occurs in the transcribed region of memory genes, but not their promoters. Thus, the regulation of histone turnover during HS memory appears tightly linked with transcription. During transcription, nucleosomes are ejected and then either directly recycled (retained) or turned over. While H3.3 recycling involves ASF1 and FACT, and is associated with H3K36me3 and H4K20 methylation (Svensson *et al*, 2015), H3.3 turnover involves UBN1 and is associated with acetylation of H4K5 and H4K12 (Verzijlbergen *et al*, 2011; Yang *et al*, 2013). Both pathways involve the HIRA complex (Jeronimo *et al*, 2019; Torné *et al*, 2020). However, these mechanisms may not be conserved in plants; while H3K36me3 is associated with H3.3 retention in other systems (Venkatesh *et al*, 2012), this function appears to have diverged in plants, as the genomic H3K36me3 pattern differs from that of H3.3 (Roudier *et al*, 2011; Sequeira-Mendes *et al*, 2014).

H3K4 hyper-methylation at HS memory-related genes depends on HSFA2 and correlates closely with transcriptional memory (Lämke *et al*, 2016; Oberkofler & Bäurle, 2022). However, while the binding of HSFA2 to memory genes drops after a few hours, the marks are maintained for several days (Liu *et al*, 2018). Our findings indicate that reduced histone turnover contributes to H3K4me3 retention and is independent of H3K4me3 levels or *HSFA2*, thus preserving high H3K4me3 levels (Fig 5C). Thus, the deposition of H3K4me3 may occur largely during the early phase and histone recycling may maintain high levels of H3K4me3 even in the absence of the HMT. H3K4me3 is generally considered a mark of recent (not present) transcriptional activity. An effect of histone turnover on the maintenance and/or spreading of histone methylation was also reported in other systems, especially for low-efficiency HMTs (Svensson *et al*, 2015; Chory *et al*, 2019; Murawska *et al*, 2021). For

instance, histone retention is required for the passage from the mono- to the di-/trimethylated state of H4K20 (Svensson *et al*, 2015). However, H3K4 trimethylation is assumed to involve highly efficient HMTs (Zentner & Henikoff, 2013; Chory *et al*, 2019). Other studies did not find a link between histone modifications and histone turnover (Ferrari & Strubin, 2015; Kassem *et al*, 2020). Our results indicate that histone H3K9 acetylation is not associated with reduced histone turnover. Acetylated histones exhibit higher turnover than non-acetylated histones, and histone deacetylation is required to reduce histone turnover in heterochromatin (Barth & Imhof, 2010; Aygün *et al*, 2013). We found no correlation between histone retention and histone acetylation, suggesting continuous acetylation and deacetylation of H3K9 of retained and new histones alike. Thus, while histone retention potentially maintains the overall modification state of histones through time, this phenomenon has different impact on different modifications, depending on their dynamic cycle of writing/ erasing. From this, we predict that H3K4 methylation will be more stable than H3K9 acetylation.

Here, we discovered a link between histone turnover and maintenance of environmentally induced histone hyper-methylation. Genes with HS-induced transcriptional memory display slower histone turnover than non-memory genes during the memory phase, providing a tentative mechanism of how high H3K4me3 levels are maintained throughout the memory phase and independently of continued *de novo* methylation. We thus unveil modified histone retention as a new regulator of plant HS memory. Future studies will reveal whether this mechanism is generally involved in transcriptional memory in response to environmental cues and whether histone retention generally contributes to the inheritance of stable epigenetic states.

Materials and Methods

Plant materials

Arabidopsis thaliana (Col-0) and *hsfa2-1* mutants (Charng *et al*, 2007) were grown on GM medium (1% glucose). Plants were grown under a 16/8 h light/dark cycle at 23/21°C. HS treatments were performed on 5-day-old seedlings by a treatment of 37°C for 60 min, 22°C for 90 min, and 44°C for 45 min.

Generation of the transgenic lines

HTR5-coding sequence was amplified from genomic DNA with primers introducing *Xma*I and *Eag*I restriction sites (Appendix Table S2). *eGFP* was amplified by introducing *Sal*I and *Xho*I restriction sites. *HTR5* and *eGFP* were fused together through a dimerized linker sequence (GACCCAGGTGCCGGAGCAGGTGCTGGA) carrying *Eag*I and *Sal*I restriction sites. The *HTR5::linker::eGFP* sequence fragment was inserted into *pBlueML2AP* vector with *Xma*I and *Xho*I to add the promoter and 3′ region of *HSP21*. Finally, the *pHSP21::HTR5::eGFP::3′HSP21* fragment was inserted using *Nco*I and *Sph*I restriction enzymes into *pGreenII* vector (Friedrich *et al*, 2021) for plant transformation. Transgenic plants were generated using the floral dip method (Clough & Bent, 1998). One single-insertion transgenic line was used for all experiments and introduced into *hsfa2-1* (Charng *et al*, 2007) by crossing and selection of doubly homozygous lines.

RNA extraction and qRT–PCR

RNA was extracted from seedlings using TRI Reagent (Sigma 93289) followed with two chloroform washes and pelleted with isopropanol overnight at −20°C. RNA was washed twice with 75% ethanol and resuspended in water. RNA samples were treated with DNAse I (Thermo Fisher 18047019) and reverse transcribed with SuperScript II (Thermo Fisher 18064014) according to manufacturer instructions. Quantification of cDNA was performed by qPCR (LightCycler480 Roche) using SYBR Green MasterMix (Promega). GFP expression was normalized on the reference gene *At4g26410* by the comparative Ct method (Appendix Table S2) (Czechowski *et al*, 2005).

Microscopy imaging

Seedlings were imaged on a Zeiss LSM880 confocal microscope.

Histone extraction and immunoblotting

Total protein was extracted from 500 mg seedlings in extraction buffer (250 mM sucrose, 60 mM KCl, 15 mM NaCl, 5 mM $MgCl_2$, 15 mM PIPES, 0.8% (v/v) Triton X-100, and Complete Mini Protease Inhibitor Cocktail (Roche)). Histones were purified from total protein extracts with 0.4 M sulfuric acid and pelleted with 12 volumes of acetone. Pelleted histones were resuspended in 100 µl loading buffer (2 M urea, 75 mM Tris pH 6.5, 0.6% (w/v) SDS, 15% (v/v) glycerol, 1% (w/v) bromophenol blue, and 0.75% (v/v) β-mercaptoethanol). Twenty microliters of histone extract was loaded per lane and separated on a 13% SDS–PAGE gel. Proteins were immunodetected with anti-GFP (Chromotek PABG1) and anti-panH3 (Diagenode C15200011) antibodies followed by goat anti-mouse Irdye 680CW (Licor 926-68070) and goat anti-rabbit 800CW (Licor 926-32211).

Chromatin immunoprecipitation

Seedlings were crosslinked under vacuum in PBS buffer with 1% (w/v) formaldehyde for 10 min on ice. Chromatin was extracted as described previously (Kaufmann *et al*, 2010). Chromatin was fragmented using a Bioruptor (Diagenode—20 cycles 30 s on/30 s off). For single ChIP, chromatin was immunoprecipitated overnight at 4°C with IgG (Thermo Fisher 026102), anti-panH3 (Diagenode C15200011), or anti-GFP (Chromotek PABG1) antibodies. Antibody–chromatin complexes were purified with Dynabeads (Thermo Fisher 10002D) and successively washed with low salt (150 mM NaCl, 1% (v/v) Triton X-100), high salt (500 mM NaCl, 1% (v/v) Triton X-100), LiCl buffer (250 mM LiCl, 1% (v/v) NP-40), and TE buffer. Chromatin was eluted with single ChIP elution buffer (1% (w/v) SDS, 0.1 M $NaHCO_3$).

For sequential ChIP, chromatin was incubated with anti-panH3 (Diagenode C15200011) or anti-GFP (Chromotek PABG1) antibodies. Antibody–chromatin complexes were treated as described above up to the elution step. Before the elution, the chromatin-bead suspensions were divided equally. One fraction was eluted with single ChIP elution buffer and kept as single ChIP control. The second fraction was eluted with sequential ChIP elution buffer (1% (w/v) SDS, 20 mM DTT) and diluted 50 times. Diluted eluates were

divided into three and incubated overnight at 4°C with IgG (Thermo Fisher 026102), anti-H3K4me3 (Abcam ab8580), or anti-H3K9ac (Abcam ab10812) antibodies and further processed as described for single ChIP. Quantification of immunoprecipitated DNA was performed by qPCR (LightCycler480 Roche) using SYBR Green MasterMix (Promega). For ChIP-seq, ChIP DNA was generated and libraries were prepared using NEBNext Ultra II FS DNA Library Preparation Kit (NEB E7645). Quality control was performed with TapeStation D1000 ScreenTape system (Agilent) and a Qubit fluorometer (Thermo Fisher). After multiplexing, samples were sequenced in paired-end mode using an Illumina NextSeq sequencer with NextSeq 500/550 Mid Output Kit v2.5 (Illumina 20024904).

ChIP-seq data analysis

Reads were mapped against the *A. thaliana* reference genome (TAIR10) using bwa mem (preprint: Li, 2013). Duplicates were removed using samtools markdup (Li *et al*, 2009). Reads for biological replicates were merged. Both individual samples and merged replicates were processed as follows. Normalized coverage tracks were generated using deeptools (Ramírez *et al*, 2016) bamCoverage (--binSize 10 --normalizeUising RPGC --extendReads). Artefactual regions identified using green screen (Klasfeld *et al*, 2022), chloroplast, and mitochondria sequences were excluded. Profiles for memory gene groups were computed using deeptools computeMatrix (scale-regions --regionBodyLength 2000 -b 1000 -a 1000). Normalized coverage profiles were plotted for individual samples and merged biological replicates by memory gene category (Friedrich *et al*, 2021). Reads mapping to the TSS + 200 bp to TSS + 700 bp regions were quantified using bedtools (Quinlan & Hall, 2010) and CPM normalized (counts per million). Empirical cumulative distribution function plots by memory gene category were generated for each sample and for averaged values over the three biological replicates. Statistical differences between memory gene groups were assessed using pairwise Kolmogorov–Smirnov test and indicated on the plots using compact letter display; different letters indicate significant differences. Visualizations were done using R/lattice (http://lmdvr.r-forge.r-project.org).

Fitting of decay functions

Raw qPCR data (*Ct* values) were pre-processed by first calculating the respective enrichment relative to the corrected input per gene:

$$Ct' = 2^{Ct_{input} - log_2 260 - Ct}. \tag{1}$$

Next, obtained values were used to calculate the ratio of enrichments between GFP and H3 for each of the compared genes and time points, as follows:

$$r_{\frac{GFP}{H3}} = \begin{cases} 0 \mid Ct'_{GFP} \leq Ct'_{lgg} \\ \dfrac{Ct'_{GFP}}{Ct'_{H3}} \mid Ct'_{GFP} > Ct'_{lgg} \end{cases}. \tag{2}$$

As a last pre-processing step, the ratio of $r_{GFP/H3}$ to the first time point (i.e., $t_0 = 4$ h) was calculated to arrive at the relative GFP to H3 ratio at time point t to time point t_0:

$$r'_{\frac{GFP}{H3},t} = \frac{r_{\frac{GFP}{H3},t}}{r_{\frac{GFP}{H3},4h}}. \tag{3}$$

The resulting values were used to fit exponential functions, $f(t)$, that describe the relative GFP to H3 ratio, N_t, at time t:

$$f(t) = N_t = N_o \cdot e^{-\mu t}. \tag{4}$$

As all ratios were scaled to the first time point, the initial ratio N_0 was set to one. The decay constants μ were estimated iteratively by minimizing the Mahalanobis distance (Mahalanobis, 1936). (D) between predicted points ($\widehat{N_t}$) and the average of measured data points ($\overline{N_t}$):

$$D = \sqrt{\left(\overline{N_t} - \widehat{N_t}\right)^T C^{-1} \left(\overline{N_t} - \widehat{N_t}\right)}, \tag{5}$$

where C is the covariance matrix of N_t. The inverse of C was obtained by singular value decomposition (i.e., pseudoinverse), since no inverse could be obtained by LU or QR decomposition. The iterative minimization was performed using the *fminsearch* MATLAB function (Natick Massachusetts: The MathWorks Inc., 2020). To avoid local minima, the fitting procedure was repeated with 50 random starting points, choosing the fit that minimizes D. The quality of the fits was assessed by the χ^2 goodness-of-fit test. Furthermore, mean squared error and final Mahalanobis distance were inspected to ensure fits of good quality.

To compare decay constants between genes, the 95% confidence intervals for the estimated decay constants were calculated by first constructing the Jacobian matrix:

$$J = \begin{bmatrix} \frac{\delta f}{\delta \mu}\Big|_{t_1} \\ \frac{\delta f}{\delta \mu}\Big|_{t_2} \\ \vdots \\ \frac{\delta f}{\delta \mu}\Big|_{t_n} \end{bmatrix}. \tag{6}$$

The variance for μ was calculated as the product of estimated variance for the whole fit,

$$\hat{\sigma}^2 = \frac{\sum_{i=1}^{m}\sum_{j=1}^{n}\left(y_{ij} - \widehat{y_{ij}}\right)^2}{n \cdot m - p}, \tag{7}$$

and the Jacobian matrix:

$$\hat{\sigma}^2_{\hat{\mu}} = \left(J^T J\right)^{-1} \cdot \hat{\sigma}^2. \tag{8}$$

The variables n, m, and p represent the numbers of time points, replicates, and estimated parameters, respectively. The 95% confidence interval was finally calculated by

$$CI_{95,\hat{\mu}} = \left[\hat{\mu} \pm \sqrt{\hat{\sigma}^2_{\hat{\mu}}} \cdot t_{0.95,nm-p}\right]. \tag{9}$$

The statistical significance of the pairwise differences between decay constants that were estimated for the considered genes was

assessed by a two-sample t-test. To this end, the calculated test statistic

$$T = \frac{\mu_1 - \mu_2}{\sqrt{\frac{\hat{\sigma}^2_{\hat{\mu}_1}}{m} - \frac{\hat{\sigma}^2_{\hat{\mu}_2}}{m}}} \tag{10}$$

was compared against the t distribution with $2m-2$ degrees of freedom. The resulting P-values were corrected for multiple hypothesis testing using the Benjamini–Hochberg procedure (Benjamini & Hochberg, 1995).

Calculation of methylation and acetylation factors

qPCR data were analyzed as described above to obtain the corrected input enrichment of all immunoprecipitation assays. Methylation factor was calculated based on

$$F = \frac{Me_{Retained} - Me_{denovo}}{Me_{t0}} \tag{11}$$

with the three quantities, $Me_{Retained}$, Me_{denovo}, and Me_{t0} calculated as follows:

$$Me_{Retained} = \frac{GFP.H3K4me3_{t=24\text{ h}}}{GFP_{t=24\text{ h}}}, \tag{12}$$

$$Me_{denovo} = \frac{H3.H3K4me3_{t=24\text{ h}} - \alpha \cdot H3.H3K4me3_{t=4\text{ h}} - GFP.H3K4me3_{t=24\text{ h}}}{H3_{t=4\text{ h}} - \alpha \cdot H3_{t=4\text{ h}} - GFP_{t=24\text{ h}}}, \tag{13}$$

$$Me_{t0} = \frac{H3.H3K4me3_{t=4\text{ h}}}{H3_{t=4\text{ h}}}, \tag{14}$$

with α representing the fraction of untagged H3 incorporated at 4 h and retained at 24 h, calculated by

$$\alpha = \left(1 - \frac{GFP_{t=4\text{ h}}}{H3_{t=4\text{ h}}}\right) \cdot \frac{\frac{GFP_{t=24\text{ h}}}{H3_{t=24\text{ h}}}}{\frac{GFP_{t=4\text{ h}}}{H3_{t=4\text{ h}}}}. \tag{15}$$

The first term in α denotes the fraction of untagged H3 at 4 h and the second term introduces the expected decay of untagged H3 from 4 to 24 h, assuming that there is no difference in decay between tagged and untagged H3.

An analogous expression was used with acetylation to calculate the acetylation factor.

Data availability

ChIP-seq data have been deposited at NCBI GEO, accession number GSE218234 (http://www.ncbi.nlm.nih.gov/geo/query/acc.cgi?acc=GSE218234).

Expanded View for this article is available online.

Acknowledgements
We thank M. Lenhard for helpful comments. We thank D. Mäker and C. Schmidt for excellent plant care. IB acknowledges funding from the European Research Council (ERC CoG 725295 CHROMADAPT). Open access funding enabled and organized by Projekt DEAL.

Author contributions
Isabel Bäurle: Conceptualization; formal analysis; supervision; funding acquisition; writing – original draft; writing – review and editing. **Loris Pratx:** Conceptualization; data curation; formal analysis; validation; investigation; visualization; methodology; writing – original draft; writing – review and editing. **Philipp Wendering:** Formal analysis; investigation; visualization; methodology; writing – review and editing. **Christian Kappel:** Conceptualization; resources; data curation; formal analysis; validation; visualization; methodology; writing – review and editing. **Zoran Nikoloski:** Formal analysis; supervision; investigation; methodology; writing – review and editing.

Disclosure and competing interests statement
The authors declare that they have no conflict of interest.

References

Aygün O, Mehta S, Grewal SIS (2013) HDAC-mediated suppression of histone turnover promotes epigenetic stability of heterochromatin. *Nat Struct Mol Biol* 20: 547–554

Barth TK, Imhof A (2010) Fast signals and slow marks: the dynamics of histone modifications. *Trends Biochem Sci* 35: 618–626

Battisti DS, Naylor RL (2009) Historical warnings of future food insecurity with unprecedented seasonal heat. *Science* 323: 240–244

Bäurle I (2017) Can't remember to forget you: chromatin-based priming of somatic stress responses. *Semin Cell Dev Biol* 83: 133–139

Benjamini Y, Hochberg Y (1995) Controlling the false discovery rate: a practical and powerful approach to multiple testing. *J R Stat Soc Ser B Stat Methodol* 57: 289–300

Brzezinka K, Altmann S, Czesnick H, Nicolas P, Górka M, Benke E, Kabelitz T, Jähne F, Graf A, Kappel C *et al* (2016) *Arabidopsis* FORGETTER1 mediates stress-induced chromatin memory through nucleosome remodeling. *Elife* 5: e17061

Brzezinka K, Altmann S, Baurle I (2019) BRUSHY1/TONSOKU/MGOUN3 is required for heat stress memory. *Plant Cell Environ* 42: 765–775

Charng YY, Liu HC, Liu NY, Hsu FC, Ko SS (2006) *Arabidopsis* Hsa32, a novel heat shock protein, is essential for acquired thermotolerance during long recovery after acclimation. *Plant Physiol* 140: 1297–1305

Charng YY, Liu HC, Liu NY, Chi WT, Wang CN, Chang SH, Wang TT (2007) A heat-inducible transcription factor, HsfA2, is required for extension of acquired thermotolerance in *Arabidopsis*. *Plant Physiol* 143: 251–262

Chory EJ, Calarco JP, Hathaway NA, Bell O, Neel DS, Crabtree GR (2019) Nucleosome turnover regulates histone methylation patterns over the genome. *Mol Cell* 73: 61–72

Clough SJ, Bent AF (1998) Floral dip: a simplified method for Agrobacterium-mediated transformation of *Arabidopsis thaliana*. *Plant J* 16: 735–743

Conrath U (2011) Molecular aspects of defence priming. *Trends Plant Sci* 16: 524–531

Conrath U, Beckers GJ, Langenbach CJ, Jaskiewicz MR (2015) Priming for enhanced defense. *Annu Rev Phytopathol* 53: 97–119

Czechowski T, Stitt M, Altmann T, Udvardi MK, Scheible WR (2005) Genome-wide identification and testing of superior reference genes for transcript normalization in *Arabidopsis*. *Plant Physiol* 139: 5–17

Deal RB, Henikoff JG, Henikoff S (2010) Genome-wide kinetics of nucleosome turnover determined by metabolic labeling of histones. *Science* 328: 1161–1164

Deaton AM, Gómez-Rodríguez M, Mieczkowski J, Tolstorukov MY, Kundu S, Sadreyev RI, Jansen LE, Kingston RE (2016) Enhancer regions show high histone H3.3 turnover that changes during differentiation. *Elife* 5: e15316

Ding Y, Fromm M, Avramova Z (2012) Multiple exposures to drought 'train' transcriptional responses in *Arabidopsis*. *Nat Commun* 3: 740

Dion MF, Kaplan T, Kim M, Buratowski S, Friedman N, Rando OJ (2007) Dynamics of replication-independent histone turnover in budding yeast. *Science* 315: 1405–1408

D'Urso A, Takahashi YH, Xiong B, Marone J, Coukos R, Randise-Hinchliff C, Wang JP, Shilatifard A, Brickner JH (2016) Set1/COMPASS and Mediator are repurposed to promote epigenetic transcriptional memory. *Elife* 5: e16691

Feng XJ, Li JR, Qi SL, Lin QF, Jin JB, Hua XJ (2016) Light affects salt stress-induced transcriptional memory of P5CS1 in *Arabidopsis*. *Proc Natl Acad Sci U S A* 113: E8335–E8343

Ferrari P, Strubin M (2015) Uncoupling histone turnover from transcription-associated histone H3 modifications. *Nucleic Acids Res* 43: 3972–3985

Friedrich T, Oberkofler V, Trindade I, Altmann S, Brzezinka K, Lämke J, Gorka M, Kappel C, Sokolowska E, Skirycz A *et al* (2021) Heteromeric HSFA2/HSFA3 complexes drive transcriptional memory after heat stress in *Arabidopsis*. *Nat Commun* 12: 3426

Goldberg AD, Banaszynski LA, Noh K-M, Lewis PW, Elsaesser SJ, Stadler S, Dewell S, Law M, Guo X, Li X *et al* (2010) Distinct factors control histone variant H3.3 localization at specific genomic regions. *Cell* 140: 678–691

Gomez-Pastor R, Burchfiel ET, Thiele DJ (2018) Regulation of heat shock transcription factors and their roles in physiology and disease. *Nat Rev Mol Cell Biol* 19: 4–19

Hilker M, Schwachtje J, Baier M, Balazadeh S, Bäurle I, Geiselhardt S, Hincha DK, Kunze R, Mueller-Roeber B, Rillig MC *et al* (2016) Priming and memory of stress responses in organisms lacking a nervous system. *Biol Rev Camb Philos Soc* 91: 1118–1133

Jaskiewicz M, Conrath U, Peterhänsel C (2011) Chromatin modification acts as a memory for systemic acquired resistance in the plant stress response. *EMBO Rep* 12: 50–55

Jeronimo C, Poitras C, Robert F (2019) Histone recycling by FACT and Spt6 during transcription prevents the scrambling of histone modifications. *Cell Rep* 28: 1206–1218

Kassem S, Ferrari P, Hughes AL, Soudet J, Rando OJ, Strubin M (2020) Histone exchange is associated with activator function at transcribed promoters and with repression at histone loci. *Sci Adv* 6: eabb0333

Kaufmann K, Muino JM, Osteras M, Farinelli L, Krajewski P, Angenent GC (2010) Chromatin immunoprecipitation (ChIP) of plant transcription factors followed by sequencing (ChIP-SEQ) or hybridization to whole genome arrays (ChIP-CHIP). *Nat Protoc* 5: 457–472

Klasfeld S, Roulé T, Wagner D (2022) Greenscreen: a simple method to remove artifactual signals and enrich for true peaks in genomic datasets including ChIP-seq data. *Plant Cell* 34: 4795–4815

Kraushaar DC, Jin W, Maunakea A, Abraham B, Ha M, Zhao K (2013) Genome-wide incorporation dynamics reveal distinct categories of turnover for the histone variant H3.3. *Genome Biol* 14: R121

Lämke J, Bäurle I (2017) Epigenetic and chromatin-based mechanisms in environmental stress adaptation and stress memory in plants. *Genome Biol* 18: 124

Lämke J, Brzezinka K, Altmann S, Bäurle I (2016) A hit-and-run heat shock factor governs sustained histone methylation and transcriptional stress memory. *EMBO J* 35: 162–175

Li H (2013) Aligning sequence reads, clone sequences and assembly contigs with BWA-MEM. *arXiv* https://arxiv.org/abs/1303.3997 [PREPRINT]

Li H, Handsaker B, Wysoker A, Fennell T, Ruan J, Homer N, Marth G, Abecasis G, Durbin R (2009) The Sequence Alignment/Map format and SAMtools. *Bioinformatics* 25: 2078–2079

Li J, Labbadia J, Morimoto RI (2017) Rethinking HSF1 in stress, development, and organismal health. *Trends Cell Biol* 27: 895–905

Liu HC, Liao HT, Charng YY (2011) The role of class A1 heat shock factors (HSFA1s) in response to heat and other stresses in *Arabidopsis*. *Plant Cell Environ* 34: 738–751

Liu HC, Lamke J, Lin SY, Hung MJ, Liu KM, Charng YY, Baurle I (2018) Distinct heat shock factors and chromatin modifications mediate the organ-autonomous transcriptional memory of heat stress. *Plant J* 95: 401–413

Lobell DB, Schlenker W, Costa-Roberts J (2011) Climate trends and global crop production since 1980. *Science* 333: 616–620

Mahalanobis PC (1936) On the generalised distance in statistics. *Proc Natl Inst Sci India* 2: 49–55

Murawska M, Greenstein RA, Schauer T, Olsen KCF, Ng H, Ladurner AG, Al-Sady B, Braun S (2021) The histone chaperone FACT facilitates heterochromatin spreading by regulating histone turnover and H3K9 methylation states. *Cell Rep* 37: 109944

Ng HH, Robert F, Young RA, Struhl K (2003) Targeted recruitment of Set1 histone methylase by elongating Pol II provides a localized mark and memory of recent transcriptional activity. *Mol Cell* 11: 709–719

Nishizawa-Yokoi A, Nosaka R, Hayashi H, Tainaka H, Maruta T, Tamoi M, Ikeda M, Ohme-Takagi M, Yoshimura K, Yabuta Y *et al* (2011) HsfA1d and HsfA1e involved in the transcriptional regulation of HsfA2 function as key regulators for the Hsf signaling network in response to environmental stress. *Plant Cell Physiol* 52: 933–945

Oberkofler V, Bäurle I (2022) Inducible epigenome editing probes for the role of histone H3K4 methylation in *Arabidopsis* heat stress memory. *Plant Physiol* 189: 703–714

Oberkofler V, Pratx L, Bäurle I (2021) Epigenetic regulation of abiotic stress memory: maintaining the good things while they last. *Curr Opin Plant Biol* 61: 102007

Ohama N, Sato H, Shinozaki K, Yamaguchi-Shinozaki K (2017) Transcriptional regulatory network of plant heat stress response. *Trends Plant Sci* 22: 53–65

Otero S, Desvoyes B, Peiró R, Gutierrez C (2016) Histone H3 dynamics reveal domains with distinct proliferation potential in the *Arabidopsis* root. *Plant Cell* 28: 1361–1371

Quinlan AR, Hall IM (2010) BEDTools: a flexible suite of utilities for comparing genomic features. *Bioinformatics* 26: 841–842

Ramírez F, Ryan DP, Grüning B, Bhardwaj V, Kilpert F, Richter AS, Heyne S, Dündar F, Manke T (2016) deepTools2: a next generation web server for deep-sequencing data analysis. *Nucleic Acids Res* 44: W160–W165

Richter K, Haslbeck M, Buchner J (2010) The heat shock response: life on the verge of death. *Mol Cell* 40: 253–266

Roudier F, Ahmed I, Berard C, Sarazin A, Mary-Huard T, Cortijo S, Bouyer D, Caillieux E, Duvernois-Berthet E, Al-Shikhley L *et al* (2011) Integrative epigenomic mapping defines four main chromatin states in *Arabidopsis*. *EMBO J* 30: 1928–1938

Rufiange A, Jacques PE, Bhat W, Robert F, Nourani A (2007) Genome-wide replication-independent histone H3 exchange occurs predominantly at promoters and implicates H3 K56 acetylation and Asf1. *Mol Cell* 27: 393–405

Schwartz BE, Ahmad K (2005) Transcriptional activation triggers deposition and removal of the histone variant H3.3. *Genes Dev* 19: 804–814

Sequeira-Mendes J, Araguez I, Peiro R, Mendez-Giraldez R, Zhang X, Jacobsen SE, Bastolla U, Gutierrez C (2014) The functional topography of the *Arabidopsis* genome is organized in a reduced number of linear motifs of chromatin states. *Plant Cell* 26: 2351–2366

Shu H, Nakamura M, Siretskiy A, Borghi L, Moraes I, Wildhaber T, Gruissem W, Hennig L (2014) *Arabidopsis* replacement histone variant H3.3 occupies promoters of regulated genes. *Genome Biol* 15: R62

Singh P, Yekondi S, Chen PW, Tsai CH, Yu CW, Wu K, Zimmerli L (2014) Environmental history modulates *Arabidopsis* pattern-triggered immunity in a HISTONE ACETYLTRANSFERASE1-dependent manner. *Plant Cell* 26: 2676–2688

Song Z, Zhang L, Han J, Zhou M, Liu J (2021) Histone H3K4 methyltransferases SDG25 and ATX1 maintain heat-stress gene expression during recovery in *Arabidopsis*. *Plant J* 105: 1326–1338

Stief A, Altmann S, Hoffmann K, Pant BD, Scheible W-R, Bäurle I (2014) *Arabidopsis* miR156 regulates tolerance to recurring environmental stress through SPL transcription factors. *Plant Cell* 26: 1792–1807

Storck WK, Abdulla SZ, Rountree MR, Bicocca VT, Selker EU (2020) A light-inducible strain for genome-wide histone turnover profiling in *Neurospora crassa*. *Genetics* 215: 569–578

Stroud H, Otero S, Desvoyes B, Ramirez-Parra E, Jacobsen SE, Gutierrez C (2012) Genome-wide analysis of histone H3.1 and H3.3 variants in *Arabidopsis thaliana*. *Proc Natl Acad Sci U S A* 109: 5370–5375

Svensson JP, Shukla M, Menendez-Benito V, Norman-Axelsson U, Audergon P, Sinha I, Tanny JC, Allshire RC, Ekwall K (2015) A nucleosome turnover map reveals that the stability of histone H4 Lys20 methylation depends on histone recycling in transcribed chromatin. *Genome Res* 25: 872–883

Torné J, Ray-Gallet D, Boyarchuk E, Garnier M, Le Baccon P, Coulon A, Orsi GA, Almouzni G (2020) Two HIRA-dependent pathways mediate H3.3 de novo deposition and recycling during transcription. *Nat Struct Mol Biol* 27: 1057–1068

Venkatesh S, Smolle M, Li H, Gogol MM, Saint M, Kumar S, Natarajan K, Workman JL (2012) Set2 methylation of histone H3 lysine 36 suppresses histone exchange on transcribed genes. *Nature* 489: 452–455

Verzijlbergen KF, van Welsem T, Sie D, Lenstra TL, Turner DJ, Holstege FCP, Kerkhoven RM, van Leeuwen F (2011) A barcode screen for epigenetic regulators reveals a role for the NuB4/HAT-B histone acetyltransferase complex in histone turnover. *PLoS Genet* 7: e1002284

Wollmann H, Holec S, Alden K, Clarke ND, Jacques P-É, Berger F (2012) Dynamic deposition of histone variant H3.3 accompanies developmental remodeling of the *Arabidopsis* transcriptome. *PLoS Genet* 8: e1002658

Yaakov G, Jonas F, Barkai N (2021) Measurement of histone replacement dynamics with genetically encoded exchange timers in yeast. *Nat Biotechnol* 39: 1434–1443

Yang X, Li L, Liang J, Shi L, Yang J, Yi X, Zhang D, Han X, Yu N, Shang Y (2013) Histone acetyltransferase 1 promotes homologous recombination in DNA repair by facilitating histone turnover. *J Biol Chem* 288: 18271–18282

Zentner GE, Henikoff S (2013) Regulation of nucleosome dynamics by histone modifications. *Nat Struct Mol Biol* 20: 259–266

Zhang C, Du X, Tang K, Yang Z, Pan L, Zhu P, Luo J, Jiang Y, Zhang H, Wan H *et al* (2018) *Arabidopsis* AGDP1 links H3K9me2 to DNA methylation in heterochromatin. *Nat Commun* 9: 4547

Zhao T, Lu J, Zhang H, Xue M, Pan J, Ma L, Berger F, Jiang D (2022) Histone H3.3 deposition in seed is essential for the post-embryonic developmental competence in *Arabidopsis*. *Nat Commun* 13: 7728

Expanded View Figures

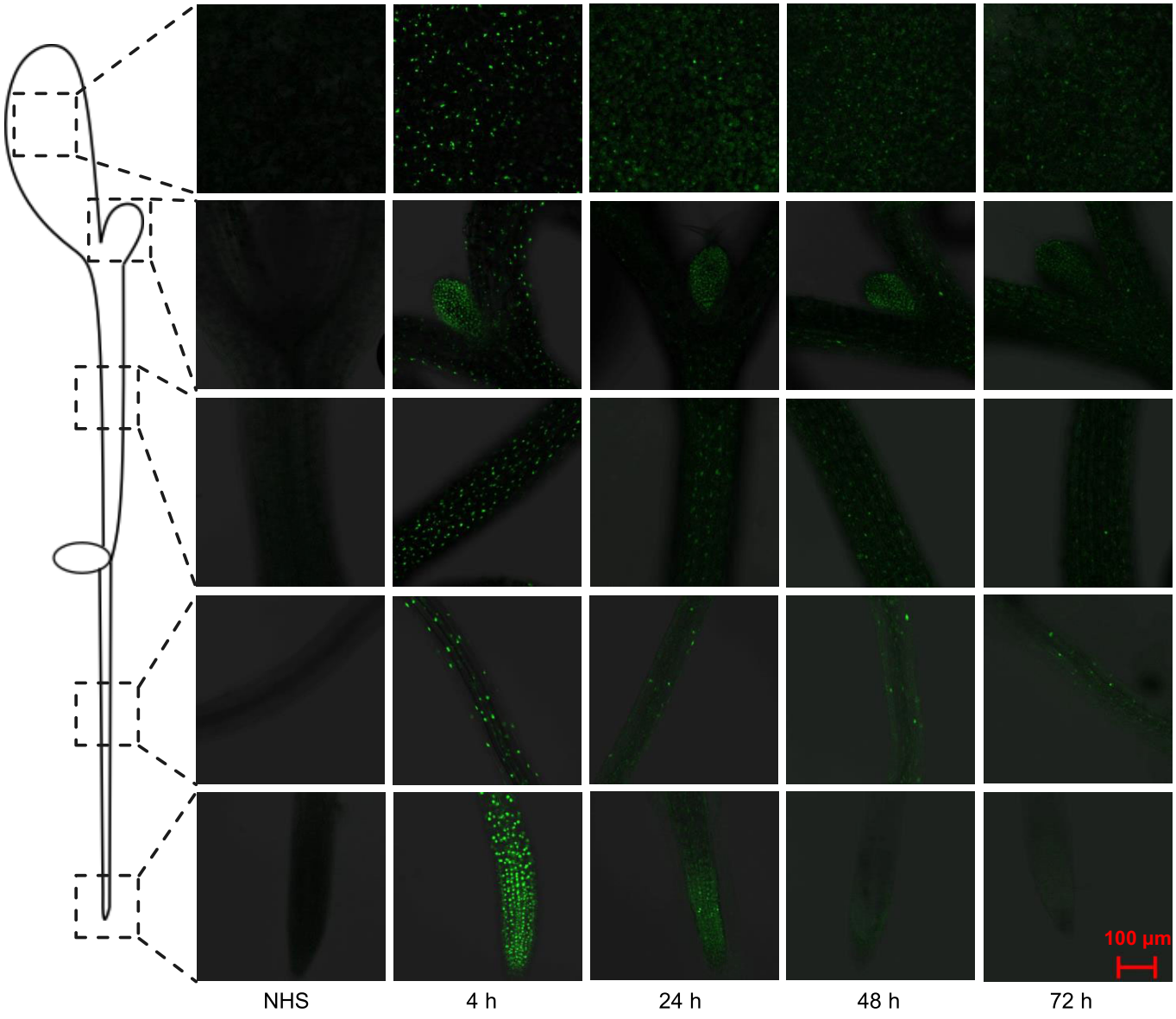

Figure EV1. Accumulation of H3.3-GFP in different organs after HS.

H3.3-GFP localizes to nuclei throughout the seedling after HS. The signal is strongest at 4 h after HS and declines thereafter. In highly dividing cells such as those in the root tip, the signal disappears more rapidly and is only present up to 24 h after HS. In non-dividing cells such as those in the elongation zone, the signal is still present at 72 h after HS. All micrographs were taken with the same settings and magnification. Size bar: 0.1 mm.

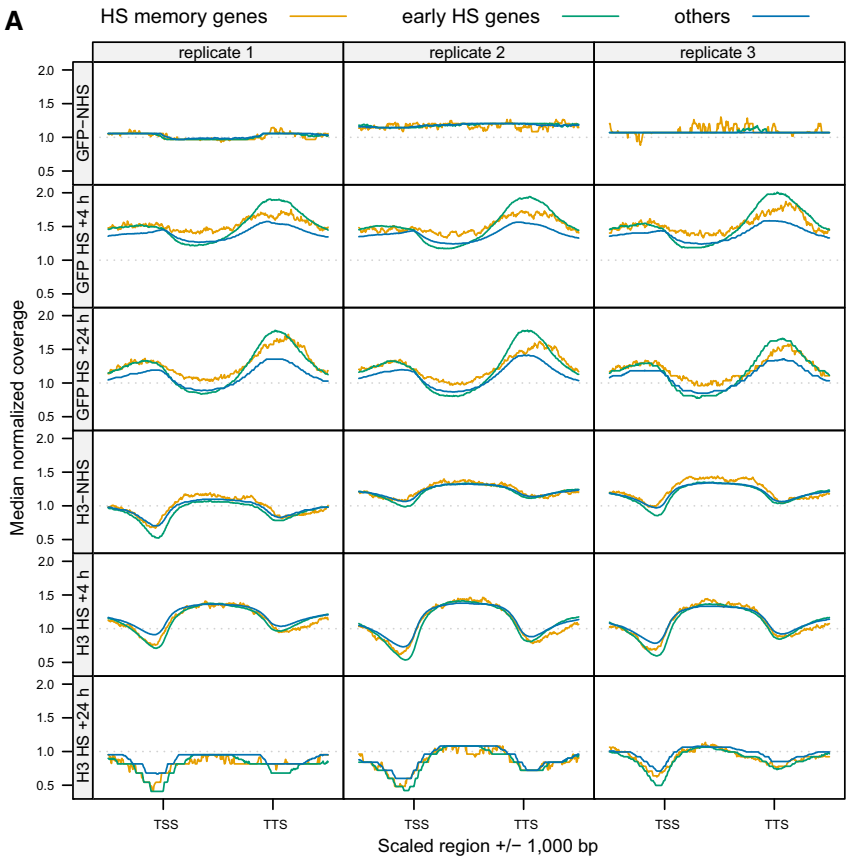

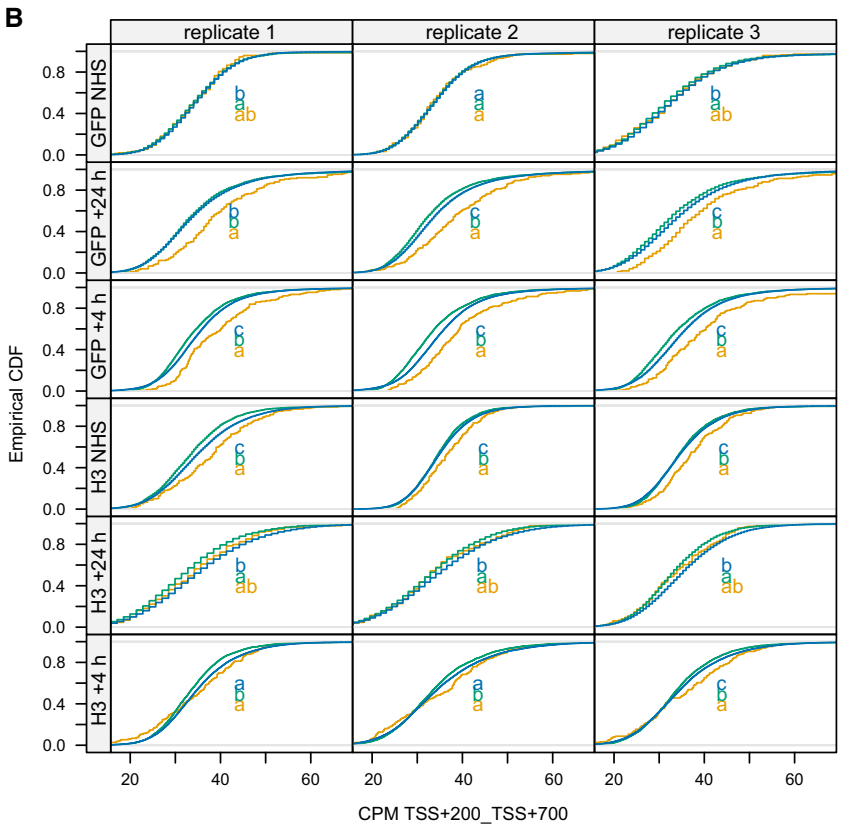

Figure EV2. Accumulation of H3.3-GFP and H3 within HS memory and non-memory genes after HS for individual replicates (cf. Fig 3).

A The global distribution of H3.3-GFP during the memory phase was determined by ChIP-seq on H3.3-GFP seedlings without HS (NHS) or 4 or 24 h after HS with anti-H3 or anti-GFP, respectively. The mean normalized coverage was plotted per replicate for H3.3-GFP (retained histones) or H3 (global pool of histones) between TSS and TTS ± 1 kb for different gene groups (HS memory genes, early HS genes, and all other genes). H3.3-GFP signal in the gene body is higher in HS memory genes 24 h after HS, but not NHS, suggesting that H3.3-GFP histones are retained during HS memory. Data are from individual replicates.

B Empirical cumulative distribution function displaying the coverage (counts per million, cpm) for the indicated groups and samples in the region TSS + 200 bp to TSS + 700 bp. Different letters indicate significant differences ($P < 0.05$, KS test). Data from three individual replicates are plotted.

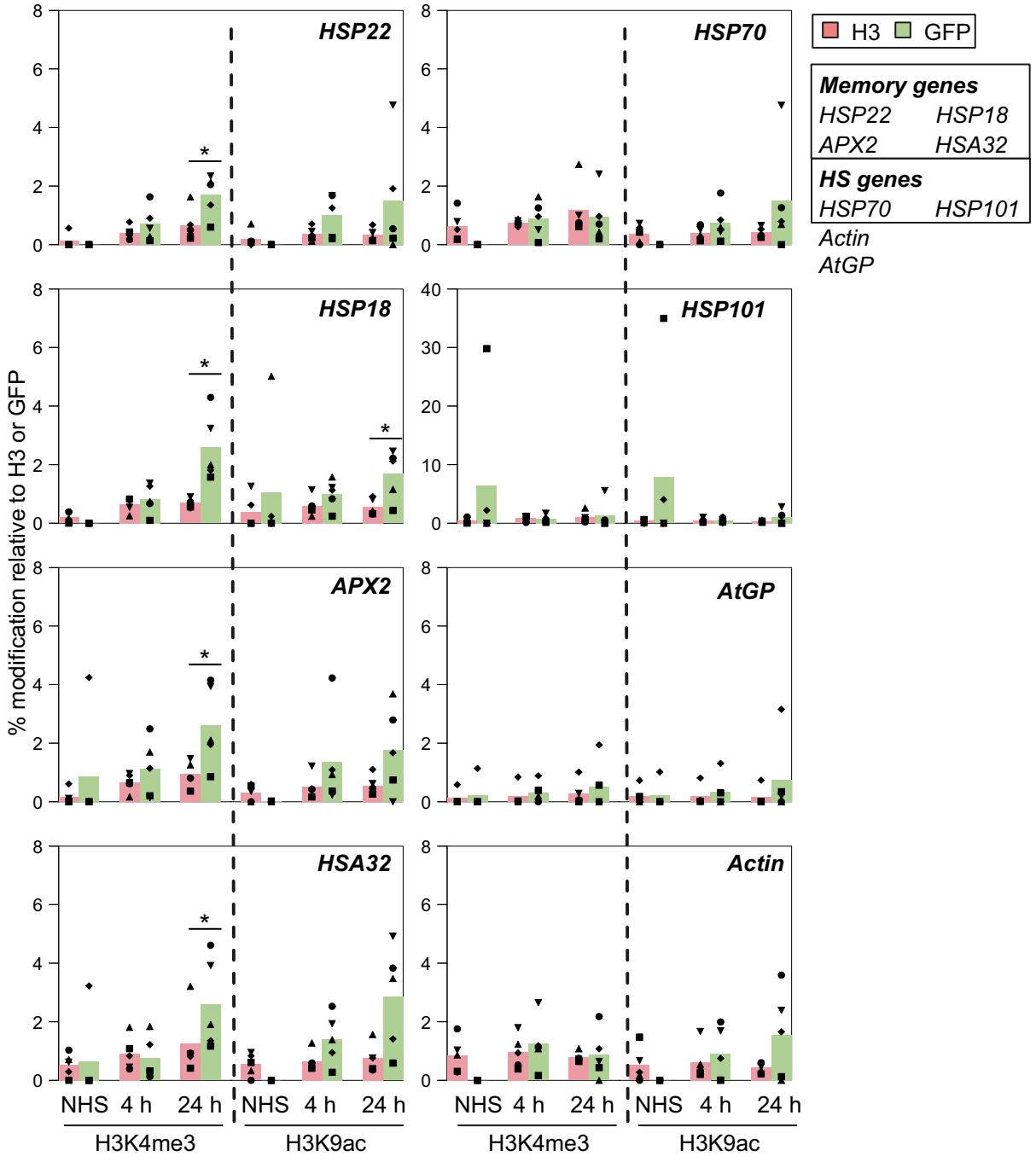

Figure EV3. HS-induced enrichment of H3K4me3 and H3K9ac on retained H3.3-GFP compared to the total pool of H3, 4 and 24 h after HS (cf. Fig 4).

Enrichment of H3K4me3 and H3K9ac on H3 incorporated during the HS response (GFP, green), and on the total histone H3 (red), respectively, at the indicated loci as determined by sequential ChIP-qPCR on H3.3-GFP seedlings without HS (NHS), or 4 and 24 h after HS, respectively. Chromatin was immunoprecipitated with anti-H3 or anti-GFP antibodies followed by anti-H3K4me3, anti-H3K9ac, or IgG (negative control) antibodies. The percentage of histone modifications among H3 or GFP was calculated and normalized on the average signal of each replicate. To control for variation in ChIP efficiency between replicates, each replicate was normalized to the average signal from that replicate (overall measured amplicons). The relative enrichment of either modification is higher in retained histones than in the total pool of histones. Data shown are means and individual data points of five biological replicates. Asterisks indicate significant differences between H3 and GFP ($P < 0.05$, Wilcoxon Mann–Whitney test).

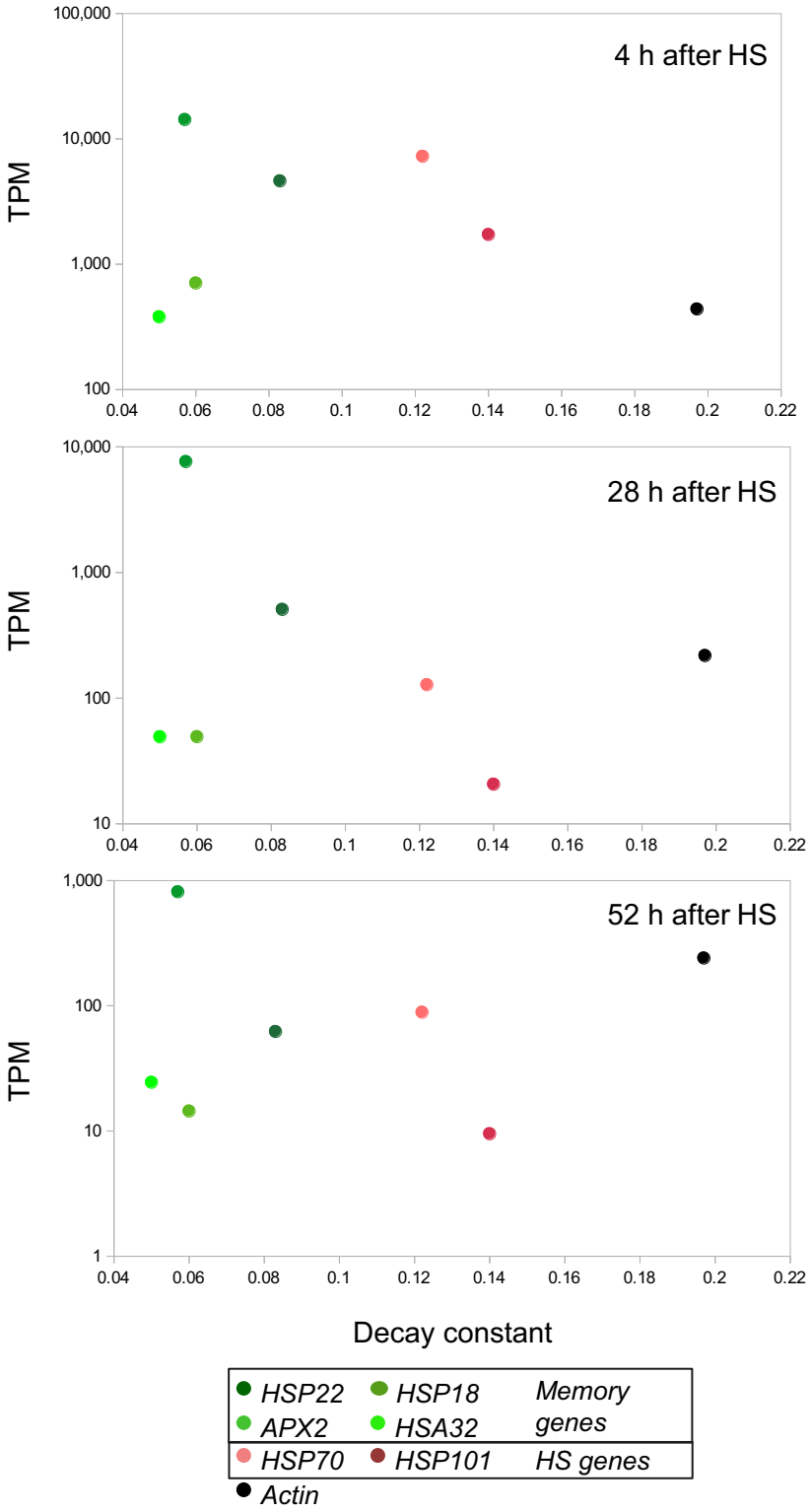

Figure EV4. Histone decay does not correlate with gene expression level after HS.

Expression values of tested genes at 4, 28, and 52 h after HS were taken from Friedrich et al (2021) and plotted against their histone decay constants. No correlation was found between histone decay and gene expression after HS.

Figure EV5. Histone retention in memory genes is independent of *HSFA2*.

H3.3-GFP association and dissociation after HS at the indicated loci as determined by ChIP-qPCR on H3.3-GFP seedlings in Col wild type or hsfa2 without HS (NHS), and 4, 12, 24, 36, 48, and 72 h after HS.

A Dynamics of H3.3-GFP enrichment relative to total H3. Data shown are means ± s.e.m. of three biological replicates.

B–D Dynamics of H3.3-GFP dissociation were evaluated by determining the percentage of GFP/H3 retained for each locus between wild type (top) and *hsfa2* (bottom). For each locus, GFP/H3 values were normalized to the 4 h value (B). The data were used to fit an exponential decay function (C), and derive dissociation constants for each locus as an estimate of histone turnover (D). Differences in histone decay between memory genes (i.e., *HSP18*$^+$, *APX2*$^+$, and *HSA32*) versus non-memory genes (i.e., *ACT*, *HSP101*, and *HSP70*) were significant in both wild type and *hsfa2*. Data shown are means of three biological replicates ± 95% confidence interval (CI). For statistical testing, 100 samples were drawn randomly from a normal distribution with mean and standard deviation of the decay constant for each gene. These data were used to perform a two-sample *t*-test.

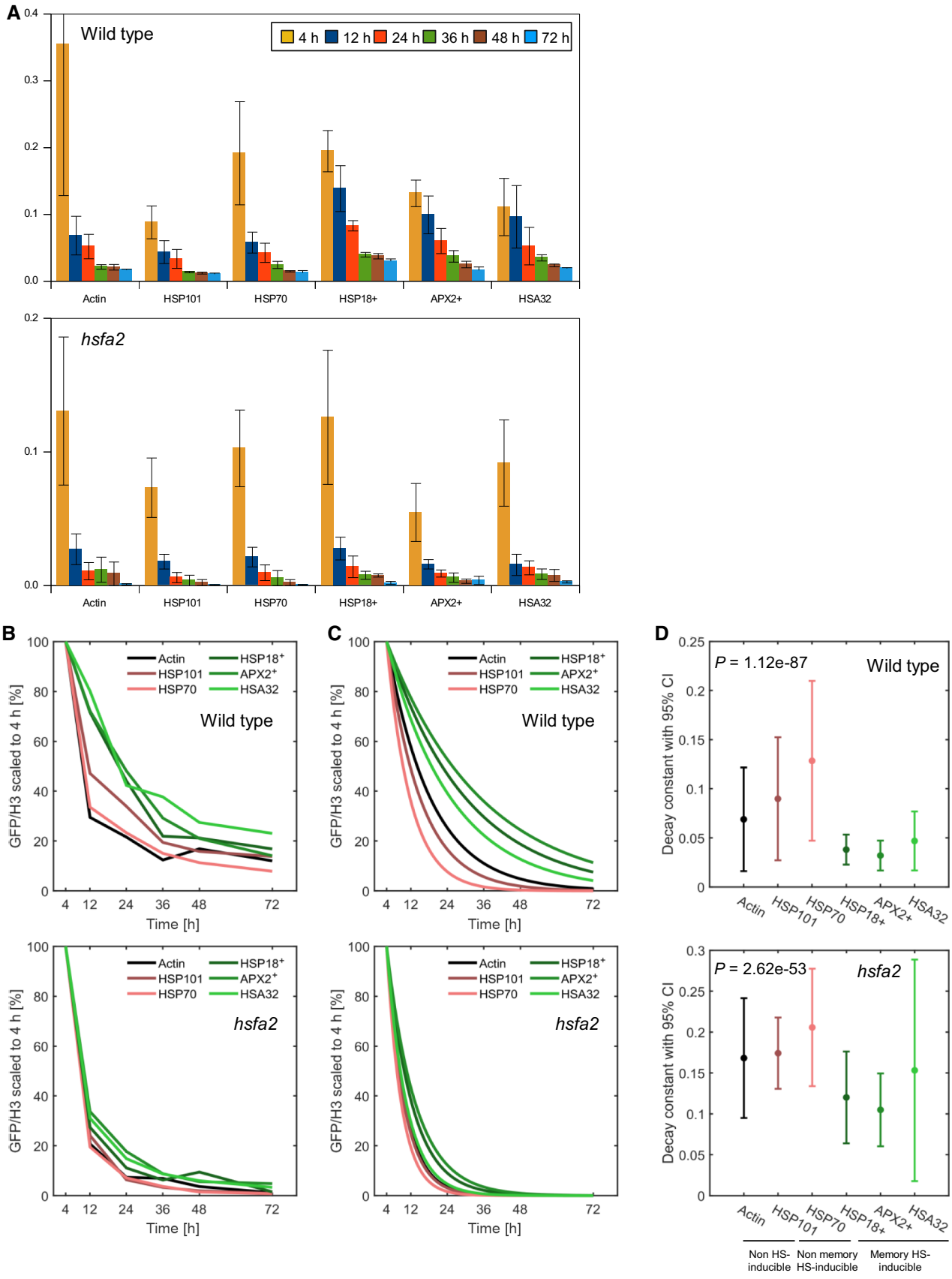
A
Wild type
4 h 12 h 24 h 36 h 48 h 72 h
hsfa2
Actin HSP101 HSP70 HSP18+ APX2+ HSA32
B
C
GFP/H3 scaled to 4 h [%]
Time [h]
Actin HSP101 HSP70 HSP18+ APX2+ HSA32
Wild type
hsfa2
D
P = 1.12e-87
P = 2.62e-53
Decay constant with 95% CI
Non HS-inducible
Non memory HS-inducible
Memory HS-inducible

Figure EV5.

Appendix for

Histone retention preserves epigenetic marks during heat stress-induced transcriptional memory

Loris Pratx, Philipp Wendering, Christian Kappel, Zoran Nikoloski, Isabel Bäurle

Table of Contents page

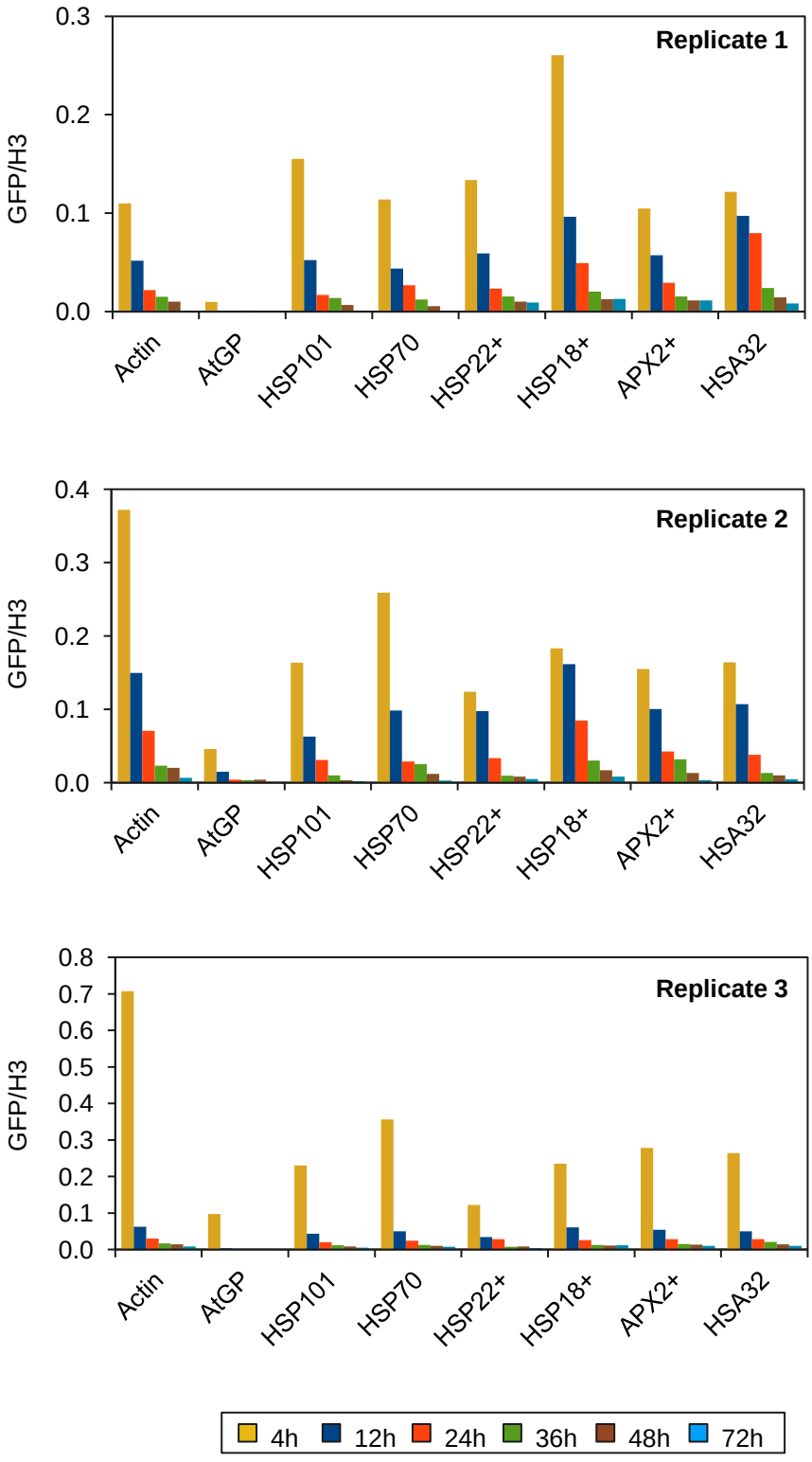

Appendix Fig S1: H3.3-GFP association patterns after HS for individual biological replicates (cf. Fig 2C).
H3.3-GFP enrichment relative to total H3 as determined by ChIP-qPCR on H3.3-GFP seedlings without HS (NHS), and 4 h, 12 h, 24 h, 36 h, 48 h and 72 h after HS at the indicated loci. Dynamics of H3.3-GFP enrichment was estimated relatively to total H3. Data of three biological replicates are shown separately.

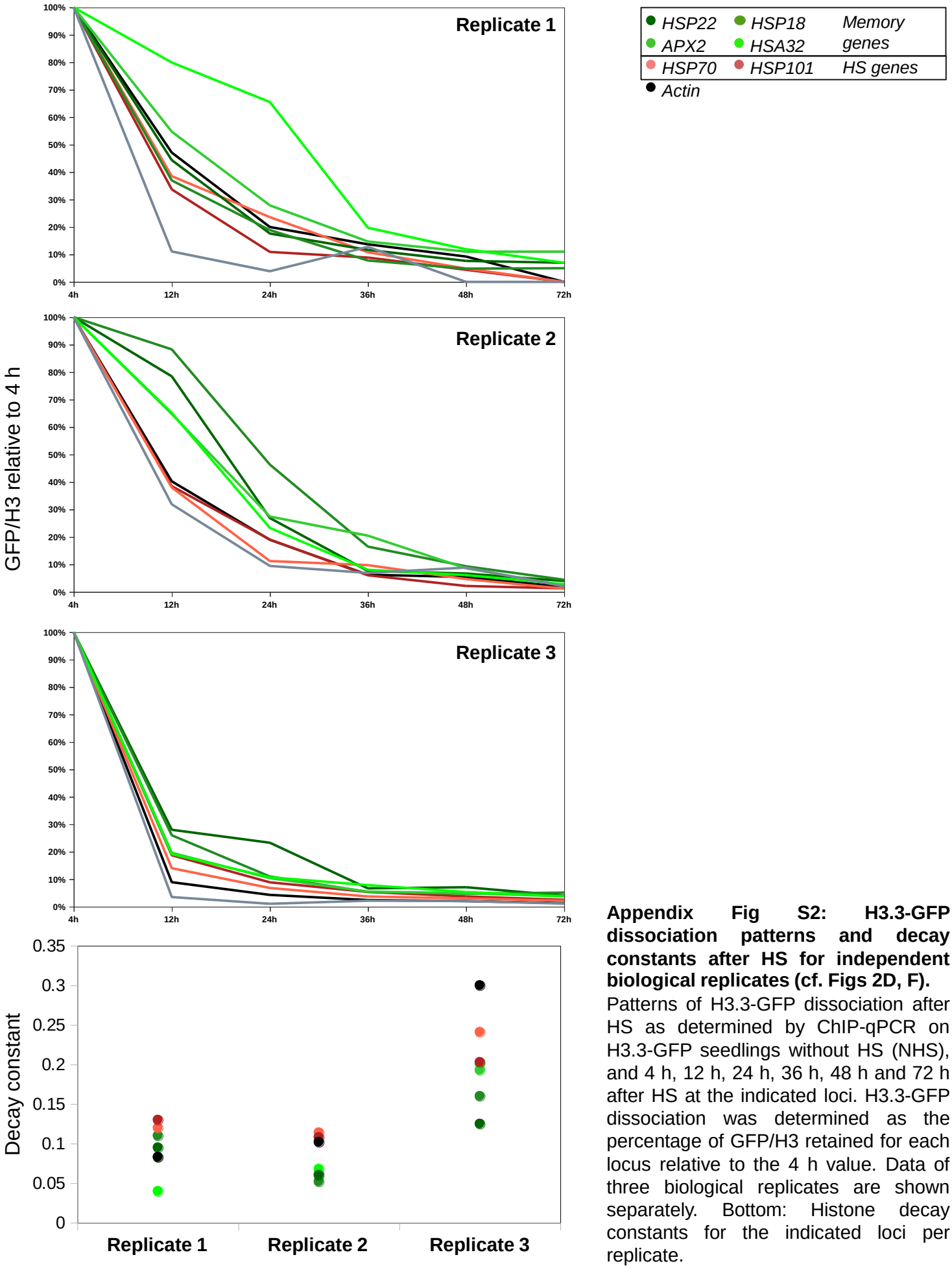

Appendix Fig S2: H3.3-GFP dissociation patterns and decay constants after HS for independent biological replicates (cf. Figs 2D, F). Patterns of H3.3-GFP dissociation after HS as determined by ChIP-qPCR on H3.3-GFP seedlings without HS (NHS), and 4 h, 12 h, 24 h, 36 h, 48 h and 72 h after HS at the indicated loci. H3.3-GFP dissociation was determined as the percentage of GFP/H3 retained for each locus relative to the 4 h value. Data of three biological replicates are shown separately. Bottom: Histone decay constants for the indicated loci per replicate.

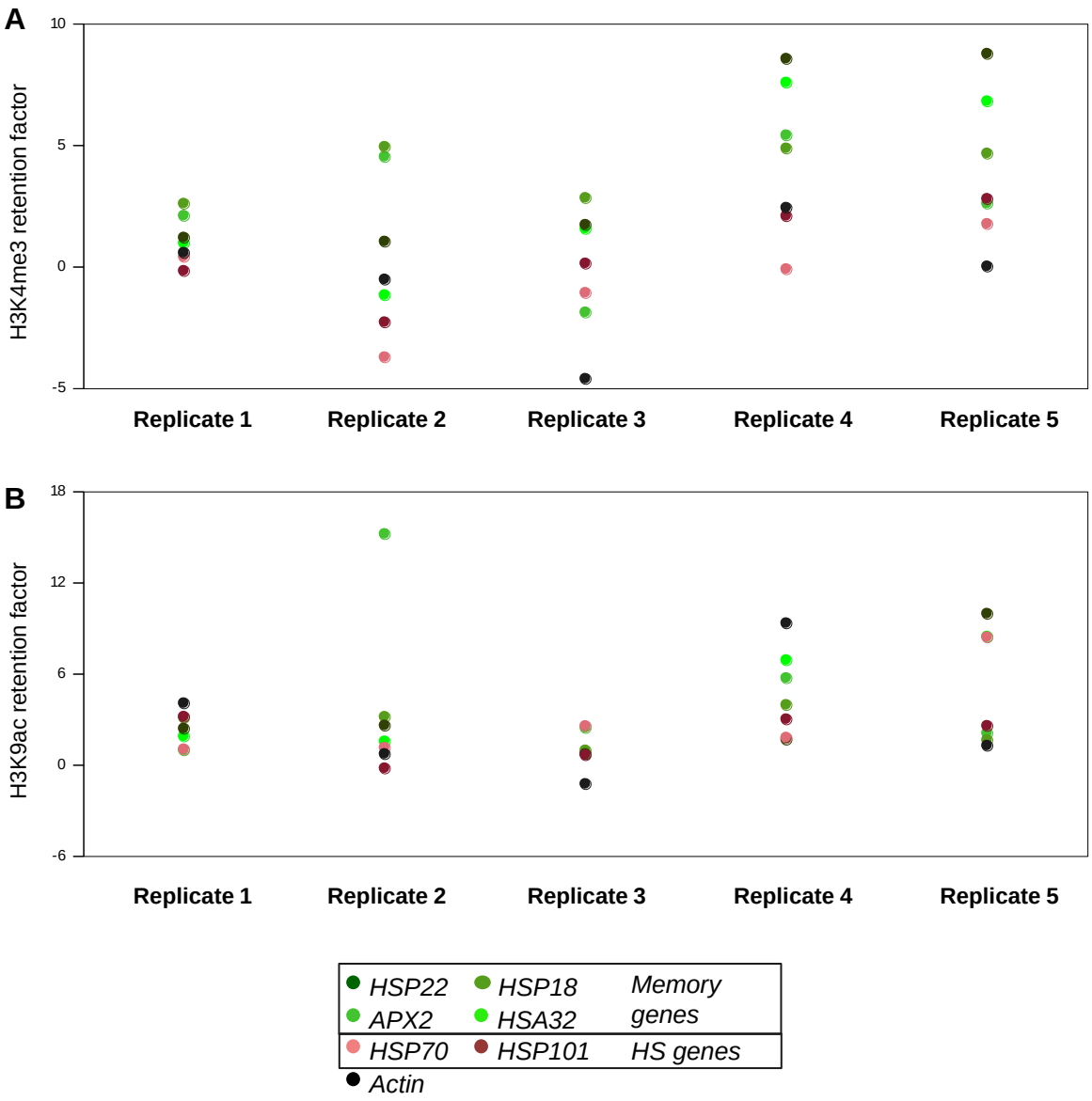

Appendix Fig S3: Histone mark retention factors for individual biological replicates (cf. Figs 5A, B).
From the enrichment of H3K4me3 (**A**) or H3K9ac (**B**) among retained (H3.3-GFP) or total histones (H3), a modification retention factor was calculated for each locus. Data of five biological replicates are shown.

Appendix Table S1: Estimated decay constant of H3.3-GFP dissociation of the 11 tested regions.

Dynamics of H3.3-GFP dissociation were evaluated by determining the percentage of GFP/H3 retained for each locus relative to the 4 h value and used to fit an exponential decay function. All loci showed a statistically acceptable fit of the model to the experimental data. se: standard error; ci_95: 95% confidence interval; D: Mahalanobis distance; mse: mean squared error; chi2: chi squared statistic.

	decay constant	s.e.	ci_95_min	ci_95_max	D	mse	chi2	p_value
Actin	0.197	0.073	0.040	0.354	0.986	0.044	1.874	0.759
AtGP	0.194	0.045	0.097	0.292	0.912	0.018	1.003	0.909
HSP101	0.140	0.022	0.093	0.187	0.685	0.011	4.826	0.306
HSP70	0.122	0.024	0.072	0.173	1.396	0.020	4.362	0.359
HSP22+	0.083	0.017	0.046	0.120	0.039	0.031	23.794	0.000
HSP18+	0.057	0.016	0.023	0.091	0.396	0.075	14.428	0.006
APX2+	0.060	0.014	0.030	0.089	0.809	0.050	0.496	0.974
HSA32	0.050	0.014	0.019	0.081	0.406	0.091	0.717	0.949

Appendix Table S2: Sequences of oligonucleotides used in this study.

3228/HTR5_CDS-XmaI-F	TAAGCACCCGGGATGGCTCGTACTAAGCAAACAG	
3225/HTR5_complete-EagI-R	TAAGCACGGCCGAGCACGTTCTCCTCTGATCCT	
3229/Linker-EagI-F	TAAGCACGGCCGGACCCAGGTGCCGGAGCAGGTGCTGGA	
3230/Linker-SalI-R	TAAGCAGTCGACTCCAGCACCTGCTCCGGCACCTGGGTC	
3233/GFP-SalI-F	TAAGCAGTCGACatggtgagcaagggcgagga	
3235/GFP-XhoI-R	TAAGCACTCGAGttataacttgtacagctcgtccatg	
796/act7_for	CGTTTCGCTTTCCTTAGTGTTAGCT	Kim et al., 2015
797/act7_rev	AGCGAACGGATCTAGAGACTCACCTTG	Kim et al., 2015
4624/AtGP1-F	ACAGTGCCACAGTTGAGCAG	Zhang et al., 2018
4625/AtGP1-R	CAGAAAAATACTCGGTGCCAAT	Zhang et al., 2018
2679/HSP101_TSS _336_F	AGCTAATCGAAGATGAATCC	Lämke et al., 2016
2680/HSP101_TSS _336_R	ATCAAAGCACCAGCTAAATG	Lämke et al., 2016
988/Hsp70_Tss+4_F	CCACTCTTCATTCATATATAAACA	Kumar and Wigge, 2010
989/Hsp70_Tss+4_R	ATTCGTCTGTGAGCTTTAAGAG	Kumar and Wigge, 2010
674/4g10250F_ATG_chip/hsp22	ATGAAGCACTTGCTAAGCATCTTC	Lämke et al., 2016
675/4g10250R_ATG_chip/hsp22	AGTCCTAATGGGATTCTCTCCA	Lämke et al., 2016
683/5g59720F_TSS+10_chip	AATCAGCAGGAAAATCAAGAAC	Lämke et al., 2016
684/5g59720R_TSS+10_chip	TCCCATAAGTCTTGCGAGAAC	Lämke et al., 2016
1854/APX2_Tss+40_F	TCGATAGGTTCTCCATTCTCTTTAGG	Lämke et al., 2016
1855/APX2_Tss+40_R	TTCCTCTTGCATCTCTGAACAGC	Lämke et al., 2016
1893/HSA32_TSS+57_F	TTCGAGAAATGTTCGATTCT	Lämke et al., 2016
1894/HSA32_TSS+57_R	CCATCTGTAGTAAGCCGCCA	Lämke et al., 2016
1259/IG5_HSP22-3kb_FWD	CGTTGGACTTGGCCTTAGAT	Lämke et al., 2016
1260/IG5_HSP22-3kb_REV	TGACTGCTCCCTGATTCTTG	Lämke et al., 2016
1255/IG3_HSP18.2-3kb_FWD	GCCCCTAGGGATTTCGACTA	Lämke et al., 2016
1256/IG3_HSP18.2-3kb_REV	CCCGTAAATAAAGCGGTCAA	Lämke et al., 2016
1857/APX2_Tss-3261_F	GGATATCAAACCCAACTTGAAGAGAG	Lämke et al., 2016
1858/APX2_Tss-3261_R	ATAATCTGAGCAAAAGATAAAACACGG	Lämke et al., 2016
6634/GFP_qRTPCR_F	ACGACTTCTTCAAGTCCGCC	
6635/GFP_qRTPCR_R	TCTTGTAGTTGCCGTCGTCC	
1547/F-AT4G26410	GAGCTGAAGTGGCTTCAATGAC	Czechowski et al., 2005
1548/R-AT4G26410	GGTCCGACATACCCATGATCC	Czechowski et al., 2005

Appendix Table S3: Number of total reads and mapped unique reads in ChIP-seq experiment.

sample	reads	mapped reads
GFP-1d-1	23298026	16775141
GFP-1d-2	31140061	23363467
GFP-1d-3	17725870	11439124
GFP-4h-1	47517979	31955767
GFP-4h-2	63243340	44072938
GFP-4h-3	34451807	20891310
GFP-NHS-1	22619897	11369549
GFP-NHS-2	43608394	12518008
GFP-NHS-3	38240676	6553841
H3-1d-1	7583474	7298377
H3-1d-2	8005598	7815154
H3-1d-3	13723007	13296911
H3-4h-1	55732879	54181109
H3-4h-2	58358634	57495558
H3-4h-3	42160952	41260240
H3-NHS-1	35669543	31900253
H3-NHS-2	60071862	56736526
H3-NHS-3	40213148	37079475